Intersonic Decohesion Along Weak Planes: Experiments and Theory

A.J. Rosakis[1] and Y. Huang[2]

[1] California Institute of Technology, Pasadena, CA, USA
[2] University of Illinois at Urbana-Champaign, Urbana, IL, USA

ABSTRACT: *Recent experimental observations of intersonic shear crack propagation, occurring in a variety of material systems, have rekindled interest in the study of the intersonic failure phenomenon. Since the early 90s, engineers and scientists working in all length scales, from the atomistic, the structural, all the way up to the scale of the earth's deformation processes, have joint efforts to study this unexplored area of fracture mechanics. The structure of the analysis presented in the article emphasizes the cooperative and complementary manner by which the experimental observations and the analytical and numerical developments have complimented each other. The article first reviews early contributions to the theoretical literature of dynamic subsonic and intersonic fracture and highlights the significant differences between tensile and shear cracks. The article then uses direct laboratory observations as a framework for discussing the physics and the mechanics of intersonic shear crack propagation occurring in constitutively homogeneous (isotropic and anisotropic), as well as in inhomogeneous systems, all containing preferable crack paths. Experiments and models are used to discuss processes such as (1) shear shock wave formation, (2) large-scale frictional contact and sliding at the crack faces, and (3) maximum attainable crack speeds and crack speed stability.*

1. INTRODUCTION

1.1 Terminology

Dynamic debonding or crack propagation result in the rapid creation of new surfaces by the breaking of bonds in a previously undamaged material. A crack tip (leading edge of a spreading displacement discontinuity) is termed supersonic, intersonic, subsonic, or simply sub-Rayleigh if its speed is compared to the characteristic wave speeds of the solid. In particular, for the simple cases of isotropic linear elastic solids, a supersonic crack tip is defined as one moving faster than the dilatational (or pressure) wave speed, c_l, of the solid. Dilatational

stress waves are equivalent to pressure waves in a gas and feature materials particle vibrations along the direction of travel of the wave. Similarly, an 'intersonic' crack is defined as one whose speed lies in the open interval between the dilatational wave speed c_l and the shear wave speed, c_s, of the solid, while a 'subsonic' crack is one whose speed is less than c_s. Shear waves feature particle motion perpendicular to their direction of travel and their speed, c_s, is typically less than twice the pressure wave speed. The exact ratio between c_s and c_l depends on the Poissón ratio of the linear elastic solid [1]. In this article, cracks propagating at exactly the dilatational wave speed will be referred to as 'pressure-sonic' (p-sonic), while the ones that move at exactly c_s will be called 'shear-sonic' (s-sonic).

Since moving cracks result in the creation of new surfaces (free or otherwise) it is perhaps not surprising that Rayleigh waves or other types of surface waves, such as Stonely waves or generalized Rayleigh waves [1], become important in their analysis. Rayleigh waves are constrained to propagate along free surfaces with a speed, c_R, which is typically equal to 87 to 95% of the shear wave speed of an isotropic linear elastic material. In this article, cracks propagating at c_R, will be referred to as 'Rayleigh cracks' while the ones propagating below c_R will be referred to as 'sub-Rayleigh'. Finally, the terminology 'superRayleigh/subshear' will be used to describe cracks that propagate in the small speed interval between c_R and c_s.

1.2 Early Work on Dynamic Fracture

As evident from Freund's [2] exhaustive monograph on the subject, the last 50 years of dynamic fracture mechanics theories have provided enormous insight into the understanding of catastrophic failure of homogeneous (monolithic) brittle solids, which is a class of materials that exhibit a linear elastic constitutive response up to failure. Early research work on dynamic fracture mechanics concentrated on materials and structures that are strictly homogeneous in nature. In other words, it has concentrated on materials that in addition to their homogeneous constitutive response they also possess strictly homogeneous fracture toughness properties thus excluding the possibility of weak paths or bonds of varying cohesive characteristics. Let us first consider Mode-I (opening) cracks propagating in homogeneous, monolithic, linear elastic solids under the action of remotely applied tractions on the boundaries. For the sake of simplicity, let us also restrict our discussion to isotropic solids.

As the remotely applied loading is increased the crack tip is typically observed to accelerate to higher speeds and it does so rather smoothly up to a speed of about 30-40% of the Rayleigh wave speed c_R. The exact percentage will, in general, depend on the details of the material's microstructure. At about these speeds, a microbranching instability sets in whereby the crack tip speed tends to oscillate and the crack follows a wavy path producing, as it attempts to branch, increasingly rough fracture surfaces. The wavy crack path, as well as the microbranching attempts, are intimately linked to a dramatic increase in size of the process region; the region of microdamage near the moving crack tip. This increase in microcrack population indicates a strong increase in fracture energy, which is required to sustain propagation at these speeds [3,4,5,6,7,8,9,10,11]. Eventually the initial mode-I crack tip branches to two or more crack paths at speeds that in a laboratory setting have never been observed to exceed 0.65 c_R. Indeed, the practical speed limit of mode-I crack growth, in purely homogeneous solids, is well below the material's Rayleigh wave speed. The reason for that is the branching instability.

As summarized by Freund [2] and Broberg [12], early theories of Mode-I crack growth have also wrestled with questions of limiting crack tip speeds within the context of homogenous linear elasticity. By assuming that an opening crack will propagate along a perfectly straight crack path, they have examined its behaviour as the crack tip increases its speed. As the crack tip speed increases, the energy flux into the crack tip decreases monotonically and eventually it vanishes at c_R. At even higher speeds no analytical solution can be found with finite and positive energy flux into the tip making superRayleigh crack growth unattainable within the confines of linear elastodynamics and singular dynamic crack growth models [2,12,13,14]. Indeed, positive energy flux into the crack tip is required to sustain cracking since crack growth involves material separation, which is inherently an energy consuming process. Hence, a necessary condition for crack growth is that energy should be supplied from the outer stress field to the crack tip region. These theoretical studies therefore conclude that the theoretical limiting crack tip speed for remotely loaded mode-I cracks in brittle solids is c_R. Such a prediction is substantially higher than the practical speed limit set by the onset of the branching instability.

The discrepancy is perhaps not so surprising if one takes a closer look at a particularly restrictive assumption that is inherent in all theoretical treatments

of the subject. As has already been mentioned, all the theoretical models so far have restricted the path of the crack tip. They prescribe a predetermined straight-line path and in so doing they disregard the physical crack's natural tendency to oscillate and eventually branch at a specific propagation speed. Thus, the analytical models approximate a very interesting, but nevertheless very different physical situation; a situation that mimics the existence of a weak plane of lower fracture toughness within the otherwise homogeneous linear elastic solid. Along this path the crack is trapped and can propagate without the possibility of activating the energy consuming process of microdamage creation, without the freedom to follow a wavy path, and without the eventual possibility of branching. The existence of such a plane (or line in a two-dimensional setting) suppresses branching and, in essence, it allows the crack to approach c_R, as is predicted by the theory.

The above interpretation of the discrepancy has clear experimental support. Specifically, Washabaugh and Knauss [15] fabricated weak planes in an otherwise homogeneous material by bonding two identical plates of a brittle polymer and then drove remotely loading mode-I cracks along the weak bond. They reported mode-I crack tip speeds approaching the polymer's Rayleigh wave speed in the limit of vanishing bond strengthen thus verifying the theoretical prediction.

The existence of weak fracture paths within solids significantly alters the initial theoretical assumption of strict material homogeneity and makes such systems very different than strictly monolithic solids. Although such materials are still homogeneous, vis a vie their constitutive properties, they are not homogeneous regarding their fracture resistance or their fracture toughness response. This is a very important distinction to bear in mind and will become even more important in the discussions throughout this article. In fact, as we have already seen, for mode-I crack growth the limiting crack tip speed for a strictly homogeneous (monolithic) solid is $0.65c_R$, or less, whereas for a solid that contains weak crack growth paths this speed is the theoretically predicted value of c_R. The differences regarding the failure of these two distinct classes of materials become even more enhanced when the possibility of shear dominated mode-II failure is considered.

Let us now consider the situation of a strictly homogeneous elastic body subjected to asymmetric dynamic loading conditions. A pre-existing stationary crack in such a body, generally speaking, would develop mixed-mode

characteristics, which evolve up to the time, of crack extension. The ratio of mode-I to mode-II, up to that time, will depend on the time history of loading and on geometry [2]. At the instant of crack initiation, time at which the crack tip ensues its movement throughout the body, the newly generated moving crack tip will not grow straight ahead of the initial stationary mixed-mode crack. Instead, the predominant theoretical belief is that it will kink and propagate at an angle to the initial crack plane: an angle that depends on the relative amount of the mode-mix (ratio of mode-II or mode-I) of its stationary predecessor. What makes this process relevant to the present discussion is the realization that this angle is also chosen to be such that the growing crack tip always maintains purely tensile (mode-I) conditions at its tip [16,17,18]. Indeed, the newly created crack tip will curve continuously, and if necessary, it will again kink abruptly to ensure that it remains a locally mode-I crack as it decohers the homogeneous materials in local tension. The natural tendency of growing cracks to propagate under strictly mode-I conditions in homogeneous monolithic solids explains the lack of interest of early engineering researchers in mixed mode, or mode-II, dynamic crack growth. In recent years this situation has changed drastically since there is an increasing demand for specialized lightweight, high-strength structures made out of inhomogeneous (heterogeneous) solids. Such solids include structural composites sandwich structures, bonded layered materials, as well as continuously graded solids. Many of these materials are composed of brittle constituents possessing substantial mismatch in wave speeds and are bonded together with weak interfaces, which frequently serve as sites for catastrophic failure. Indeed, many of these solids are designed for applications involving either anticipated or accidental impact loading. The existence of interfaces in this new generation of structural materials has refocused the attention of engineers to the problem of dynamic crack growth along predetermined crack paths that are often identified as the boundaries between the phases of heterogeneous solids. Forcing a crack to propagate dynamically along a specific path and thus removing its freedom to choose a path that will allow it to remain locally mode-I, results in a number of very interesting phenomena, some of which will be discussed in this article. In fact, mixed mode or mode-II growing cracks in inhomogeneous solids exhibit behaviours that are very different than their mode-I counterparts. As we will see in the following sections, such behaviours include the possibility of intersonic and even supersonic crack tip speeds, as well as the likelihood of

large-scale dynamic frictional contact and dissipation of the crack faces. Finally, they often feature the radiation of shock wave-like discontinuities from the crack tips and from the ends of the contact zones.

In the present article, the reader's attention is focused on shear dominated cracks or debonding forced to propagate along weak planes at the interface between linear elastic solids. For simplicity, the article's point of view, theoretical or experimental, will remain a two-dimensional one. A brief review of the theoretical literature on the subject will first be presented. Then, the article will concentrate on the question of the attainability of intersonic crack tip speeds. The discussion will revolve around the presentation and analysis of laboratory evidence of intersonic crack growth in different material systems involving similar isotropic or anisotropic constituents that are separated by weak interfaces. The discussion will not follow the proper chronological order of research discoveries. Rather, it will center around two distinct classes of bonded material systems: one involving identical isotropic constituent solids and the other involving simple anisotropic solids. A brief discussion of bimaterial systems involving highly dissimilar constituents will also be presented.

2. CRACK PROPAGATION IN WEAK PLANES BETWEEN TWO CONSTITUTIVELY HOMOGENEOUS, ISOTROPIC SOLIDS

When the crack tip speed, v, is subRayleigh ($0<v<c_R$) the asymptotic stress field is square root singular (as it is in the equivalent mode-I problem). The near tip stress components, σ_{ij}, viewed from a local coordinate system which is propagating with the crack tip at speed v, have the following form:

$$\sigma_{ij}(\eta_1,\eta_2) = K_{II}^{d}\,\frac{f_{ij}(\theta,\alpha_l,\alpha_s)}{\sqrt{r}}, \tag{2.1}$$

where (η_1,η_2) are the coordinates of a point with respect to this moving Cartesian coordinate system (the η_1-axis lies along the direction of crack growth and the η_2-axis is perpendicular to the crack plane), r is the distance to the moving crack tip, $f_{ij}(.,.)$ are known functions of crack tip speed v and

angular position θ, the indices *ij* have the range of 1,2, while the variables α_l, and α_s are defined (Freund, 1990) as follows:

$$\alpha_l = \sqrt{1 - \frac{v^2}{c_l^2}},\ \alpha_s = \sqrt{1 - \frac{v^2}{c_s^2}}\ , \tag{2.2}$$

where c_l and c_s are the longitudinal and shear wave speeds, respectively. As it is evident from the general form of this solution, the stress tensor features a square root singularity with respect to *r* and has a amplitude factor, K_{II}^d, which in turn is called the mode-II dynamic stress intensity factor and is itself expressible in the form:

$$K_{II}^d = k(v) K_{II}^S\ . \tag{2.3}$$

The factor $k(v)$ above is a universal function of crack tip speed and K_{II}^S is the stress intensity factor of an equivalent stationary crack at the same instantaneous location as the growing crack [2,12]. K_{II}^S is independent of a crack tip speed and it is an unknown function of external loading and geometry. The function $k(v)$, on the other hand, is known. When $v = 0$ its value is equal to 1, while it monotonically decreases to zero as $v = c_R$. The above asymptotic solution allows the evaluation of the dynamic energy release rate, G, which represents the energy flux into the crack tip singularity, per unit of new crack area (per unit new area of sliding for mode-II cracks). This is given by:

$$G = A_{II}(v) \frac{(K_{II}^d)^2}{E'}, \tag{2.4}$$

where E' is an equivalent Young's Modulus of the solid ($E' = E$ for plane stress, $E' = E/(1-\nu^2)$ for plane strain, ν is Poissón's Ratio) and $A(v)$ is an increasing function of speed such that $A(0) = 1$ and $A(v) \to \infty$ as $v \to c_R$ [2]. By substituting equation (2.3) into equation (2.4) the dynamic energy release rate G (energy supplied into the tip) can now be expressed in the following separable form:

$$G = g(v)\frac{(K_{II}^{S})^2}{E'}, \tag{2.5}$$

where $g(v) = A(v)k^2(v)$ and is a function that exclusively depends on the crack tip speed and the elastic material properties. At this point it is very important to note that although $A(v)$ and $k(v)$ are monotonic functions that have opposite behaviour as $v \to c_R$ [$A(v)$ becomes unbounded while $k(v)$ vanishes], the combination $g(v) = A(v)k^2(v)$, nevertheless, vanishes at this limit. In fact, $g(v)$ decreases almost linearly from 1 to 0 as the crack speed increases from 0 to c_R. The form of equation (2.5) and the properties of $g(v)$ have strong physical consequences. They imply that the energy supplied to the crack tip remains finite and positive throughout the subRayleigh regime and it vanishes only as the crack speed reaches c_R. The above provide a strong indication that subRayleigh cracks will have a hard time to smoothly propagate past c_R, unless some other mechanism is identified which allows for such a transition. Indeed, according to the steady-state model, if one now looks for singular crack growth solutions at the small speed interval between c_R and c_S, the energy supplied to the tip becomes negative thus excluding, in that interval, steady-state crack growth [2,12]. Obviously, transient crack growth past that interval is not excluded by the above discussion since so far the arguments are made on the basis of a strictly steady-state model. In fact, the cracks may conceivably jump discontinuously from one speed regime to the other without smoothly accelerating through a forbidden region. Cracks may also nucleate spontaneously and grow as intersonic cracks without ever being subsonic. Considering the above, the quest for intersonic possibilities is still justifiable.

2.1 Early Models of Intersonic Shear Crack Propagation

Let us now turn our attention to the few early theoretical studies of intersonic shear crack propagation. In particular, let us first consider a semi-infinite mode-II crack propagating at a constant speed, *v*, along a predetermined straight-line crack path which models a weak bond between two identical isotropic linear elastic solids. This is a purely steady-state elastodynamic problem whose mode-I counterpart has already been discussed in the introduction. This problem was first analyzed by Freund [2,19] who concentrated on intersonic crack growth in

linear elastic solids and commented on the remarkable changes that the asymptotic stress and particle velocity fields experience as the crack tip speed crosses different possible speed regimes. Looking for solutions in the intersonic crack tip speed interval $(c_s < v < c_l)$, Freund [19] was able to reveal the existence of a singular stress field that was drastically different than its subsonic counterpart. The mathematical reason for the difference is the change in nature of the governing differential equations of two-dimensional plane elastodynamics; a change that occurs as the crack speed moves from the subsonic to the intersonic regime. Indeed, whereas in the subsonic case the steady-state problem involves two elliptic partial differential equations governing the two scalar elastic potential functions, in the intersonic regime it involves one elliptic and one hyperbolic equation. The elliptic equation governs the dilatational potential while the hyperbolic one governs the shear potential. This allows for the possibility of 'characteristic' lines, somehow related to shear deformations. The physical meaning of such lines will become apparent in the following discussion.

If one follows the above conventions and notation in relation to the subsonic crack tip stress field, and if one employs a Cartesian coordinate system (η_1,η_2) translating with the crack tip and oriented as shown in figure 1, the intersonic asymptotic field for $c_s < v < c_l$ takes the form:

$$\sigma_{ij}(\eta_1,\eta_2) = K_{II}^{*}\left\{\frac{l_{ij}(\theta,\alpha_l,\hat{\alpha}_s)}{r^q} - \frac{m_{ij}(\alpha_l,\hat{\alpha}_s)}{(-\eta_1-\hat{\alpha}_s|\eta_2|)^q}H(-\eta_1-\hat{\alpha}_s|\eta_2|)\right\}, \quad (2.6)$$

where $l_{ij}(.,.)$ is a known function of scaled angular position θ and speed through the relativistic functions α_l and $\hat{\alpha}_s$ and $m_{ij}(.,.)$ is a known function of only speed. $H(.)$ is the Heaviside step-function and q is the singularity exponent, which is a function of crack tip speed given by:

$$q(v) = \frac{1}{\pi}\tan^{-1}\frac{4\alpha_l\hat{\alpha}_s}{(1-\hat{\alpha}_s^2)^2}. \quad (2.7)$$

The variable α_l is defined in equation (2.2) above while $\hat{\alpha}_s$ is given by:

$$\hat{\alpha}_s = \sqrt{\frac{v^2}{c_s^2} - 1}\,. \tag{2.8}$$

The coefficient K_{II}^*, which represents a common amplitude factor to all stress components, is called the intersonic mode-II stress intensity factor and it is equivalent to K_{II}^d of the subsonic solution. This amplitude is not determined by the asymptotic solution. Rather it depends, in general, on the transient loading and on geometry [2].

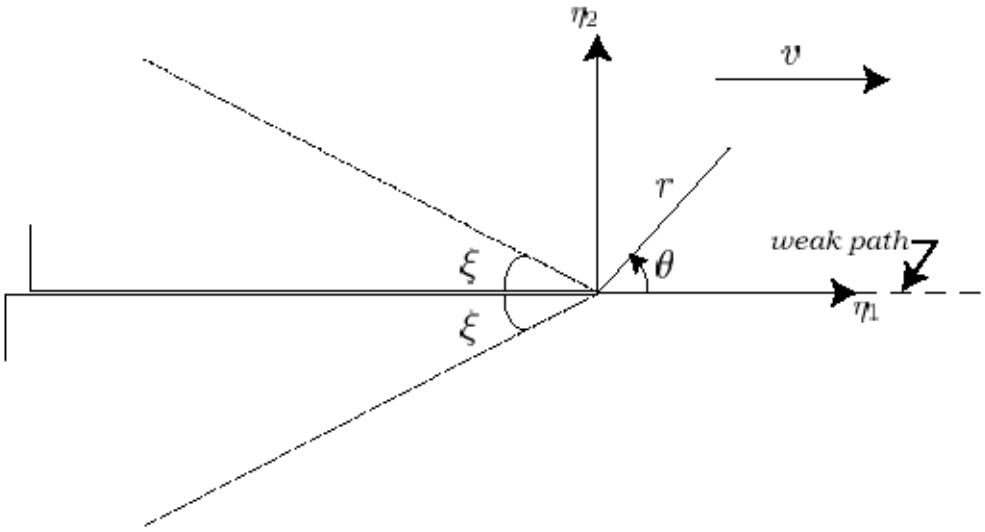

Figure 1: An intersonic mode-II crack confined to grow along a straight-line path in an isotropic solid. The illustration shows the crack tip coordinate system and two Mach lines radiating from the crack tip.

From the Heaviside function that appears in equation (2.6) we clearly see that the asymptotic solution predicts two traveling stress discontinuities (Mach waves) attached to the shear crack tip and inclined at an angle $\xi = \sin^{-1}(c_s / v) = \tan^{-1}(1/\hat{\alpha}_s)$ to the crack faces as evident from by the

argument of the step function. These stress discontinuities are schematically indicated in figure 1. The stresses are singular not only at the crack tip, but also along the two Mach fronts with the same order of singularity as that of the crack tip. That means that the crack tip singularity is 'radiated' out along the Mach lines which are 'characteristics' arising from the hyperbolic nature of the partial differential equation that governs the shear elastic potential in the intersonic regime. Across the Mach front, the normal stress and the normal particle velocity perpendicular to the front are continuous, whereas the shear stress and tangential velocity suffer an infinite jump. Hence these fronts are shear Mach waves. Another major difference of intersonic crack growth from the subRayleigh crack behavior lies in the nature of the stress singularity exponent q. In the intersonic regime the singularity exponent is not equal to 1/2. Instead, it is a strong function of crack tip speed and its variation is plotted in figure 2 for both the plane stress and plane strain cases and for a value of Poissón's Ratio ν of 0.34. The figure shows that q increases monotonically with speed from a value of 0 at c_s to a value of 1/2 at a speed of $\sqrt{2}c_s$ and thereafter, as the crack approaches the dilatational wave speed c_l it decreases monotonically to 0. The fact that the strength of singularity is drastically reduced compared to the classical square root behaviour of the subRayleigh regime has direct consequences to the energetics of crack growth. In fact, the strongest consequence of that is the fact that dynamic energy release rate G, or equivalently the energy supplied to the shear crack tip per unit slip area increment, is identically zero in the intersonic interval except at one distinct crack tip speed. This speed is equal to $\sqrt{2}c_s$ and corresponds to a value $q = 1/2$. At that speed, the intersonic crack tip recovers the square-root singular nature, and as the functions $m_{ij}(\alpha_l, \hat{\alpha}_s)$ in equation (2.6) vanish, the shear Mach waves disappear. In addition, the energy supplied to the tip is no longer zero and has a positive finite value equal to:

$$G = \frac{\left(K_{II}^{*}\right)^2}{4\mu\alpha_l}, \tag{2.9}$$

where μ is the shear modulus of the isotropic linear elastic solid [19].

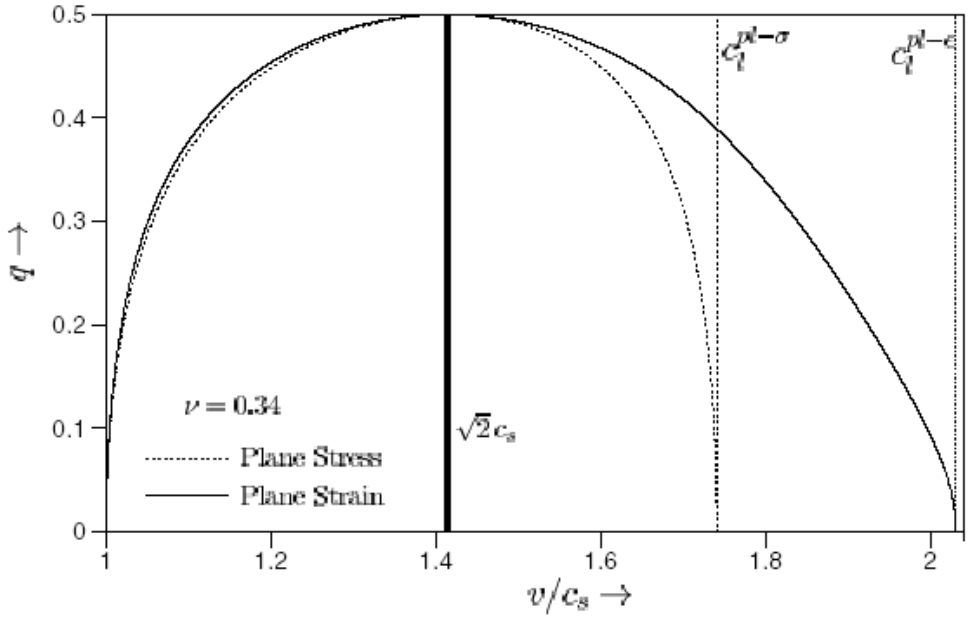

Figure 2: The variation of the mode-II crack tip singularity exponent with crack speed.

The implications of the above observations for the ability of a shear crack to propagate intersonically have first been discussed by Freund [19] and later on by Broberg [13,14]. As they point out, within the confines of the singular elastodynamic analysis discussed above, a shear crack can definitely propagate intersonically at the interesting crack tip speed of $\sqrt{2}c_s$, where finite and positive energy flux is available to it. In all other intersonic speeds the situation remains uncertain. At such speeds, *G* is identically zero which, although is not as prohibitive as is the negative value predicted for the superRayleigh/subsonic interval, it is, nevertheless, discouraging from the point of view of singular elastodynamics.

Following the above discussion, it is obvious that the theory does not exclude intersonic shear crack growth, as it clearly did for the mode-I discussed in the introduction. However, the theory is unable to conclusively predict whether the occurrence of such a phenomenon is likely or even possible. As

emphasized by Freund [2,19] and Broberg [13,21,22] in most of their work on the subject, the idealization of the crack tip process zone to a point-size dissipative tip (the singular crack tip), results in a physically unrealistic situation whereby the requirement of a positive energy flux to the crack tip is met only at $\sqrt{2}c_s$. As a consequence, non-singular, cohesive zone models in which the crack tip region is permitted to assume a finite extent might allow for non-zero flux throughout the intersonic regime. In addition, the possibility of theoretically addressing the problem of the smooth crossing of the forbidden superRayleigh/subshear interval requires the relaxation of the steady-state assumption. In so doing, there is some hope that a transient mechanism which would facilitate the transition from subRayleigh to intersonic, could be identified. Obviously, the possibility of achieving both such goals analytically is slim, whereas early numerical studies have indeed managed to provide us with the means of analyzing such issues.

In perhaps the first transient analytical study of shear crack propagation ever reported, Burridge [23] employed a simple form of frictional, cohesive zone model to analyze the problem of a mode-II crack-like entity propagating along an interface between two identical half spaces. The crack was allowed to grow in a self-similar manner from zero initial length along the interface. The two half spaces were subjected to uniform normal and shear tractions and were held together by Coulomb friction. In effect, this problem represents the limiting case of a shear crack of zero cohesive energy together with a finite cohesive strength.

For cracks propagating with high subRayleigh speeds, Burridge was able to identify a peak in shear stress propagating ahead of the main crack. This peak was observed to increase in magnitude as the main crack tip speed approached c_R. He then postulated that if this stress peak exceeds the limiting static friction then a secondary micro-crack may nucleate and may grow ahead of the main crack. The main crack may continue to move at the Rayleigh wave speed, provided that the cohesive strength is sufficiently high. Otherwise it joins up with the microcrack and the resulting combination may accelerate and propagate at a speed close to c_l. By using a finite difference scheme, Andrews [24] analyzed the transient problem of the symmetric expansion of a mode-II crack propagating along a prescribed path under the action of a uniformly applied remote shear stress. Rupture at the crack faces was resisted by a slip

weakening cohesive zone of the type described by Ida [25] and by Palmer and Rice [26]. Andrews collaborated Burridge's analytical prediction and he found that the expanding shear crack accelerates to speeds close to c_R and induces the nucleation of a secondary slip region propagating just in front of it. This was found to be possible provided that the limiting static friction was not high enough. This secondary crack zone coalesces with the main crack and the combination was found to propagate at about speeds $1.5c_s$; a value that is surprisingly close to the special speed of $\sqrt{2}c_s$ described by Freund's analysis [19]. His numerical observations together with the study by Burridge [23] describe one possible mechanism which would allow a subsonic crack to cross the forbidden speed regime between c_R and c_s. For the remainder of this article this mechanism will be referred to as the 'Burridge-Andrews Mechanism'.

Andrews [24] pointed out that for intersonic cracks, where the crack tip singularity is less than 1/2, a non-zero fracture energy is supported only when the stress drop is not abrupt, i.e. when the crack tip region is allowed to have a finite extent. Das and Aki [27] used a boundary integral method to study the transient mode-II crack expansion in an infinite, linear elastic isotropic solid subjected to remote shear stress. The crack tip in this study was modeled as a structureless point and dynamic friction was assumed to act along the crack faces. Using a critical stress criterion, they confirmed the numerical results of Andrews [24]. The subsequent numerical studies by Day [28] and Johnson [29], who examined various aspects of intersonic crack, also confirmed the importance of the stress peak traveling with the shear wave speed in facilitating the subRayleigh to intersonic transition. The Burridge-Andrews Mechanism was found to be activated in a variety of situations and thus became a widely accepted interpretation. The stability of a semi-infinite steady-state mode-II crack, confined to propagate along a straight-line path under the action of a point load at a finite distance from the crack tip was first studied by Burridge *et al.* [30]. This work assumed the presence of a slip-weakening cohesive zone resisting crack advance and concluded that the crack is inherently unstable in the entire subRayleigh regime. When propagating intersonically, the crack was found to be unstable in the open speed interval between c_s and $\sqrt{2}c_s$ and

stable when v lies in the closed interval between $\sqrt{2}c_s$ and c_l. The open speed interval between c_R and c_s was confirmed to be forbidden.

Extensive analytical contributions into the cohesive modeling of shear crack have been presented by Broberg [20,31]. He considered the problem of a self-similar intersonic mode-II crack expanding symmetrically from zero initial length under the action of a remote uniform shear stress. By assuming a Barenblatt process region he was able to show that the energy supplied to the crack tip, G, remains positive and finite during intersonic crack growth. At the same time, he was able to demonstrate that G depends on the extent of the process zone as:

$$G = f(v)(\tau_\infty^2 a / \mu)(L/a)^{1-2q} \tag{2.10}$$

where L is the length of the process zone, a is the crack length, $f(v)$ is a complicated function of a crack tip speed and $q(v)$ is the speed-dependent crack tip singularity shown in figure 2. The dependence of G on L/a, for the limit of a vanishing normalized process zone length, $L/a \to 0$, shows that the energy supplied to the crack tip vanishes at all intersonic speeds with the exception of $v = \sqrt{2}c_s$ which is the speed for which $q = 1/2$. This observation is consistent with the results of the purely singular (structureless) analysis of Freund [19] who predicted G to be identically zero at all speeds with the exception of $v = \sqrt{2}c_s$ where G remained finite and positive. For cases when the process zone length may not be neglected, numerical evaluation of equation (2.10) reveals that the energy flux increases from zero at $v = c_s$ to a maximum value at a speed somewhat lower than $\sqrt{2}c_s$ and then vanishes again at $v = c_l$. The exact location of this maximum is dependent on L/a and moves to $\sqrt{2}c_s$ as $L/a \to 0$. In expanding the above analysis, Broberg also considered the requirement of a constant critical fracture energy, G_c, balancing the available energy flux. In so doing, he effectively imposed a criterion for intersonic growth. He showed that under these conditions the crack would accelerate from a speed close to that corresponding to the maximum value of G all the way up to the dilatational wave speed c_l. In a later contribution he also solved the transient problem of an accelerating semi-infinite intersonic mode-II crack [12].

2.2 Laboratory Evidence of Intersonic Shear Crack Propagation

The experimental results of this section can be better understood with the above discussion in mind. The theoretical models of intersonic shear crack propagation presented in section 2.1 illuminate the crucial points that are central to our understanding of the experimental observations.

The first point involves the identification of 'permissible' and 'forbidden' crack tip speed regimes during dynamic shear crack propagation. In this regard, the small speed regime between c_R and c_S is identified as being forbidden while purely subsonic and intersonic crack propagation is theoretically plausible.

The second point is related to the identification of a mechanism that could allow an intersonic crack to transit through the forbidden regime. Here two possibilities seem to emerge. A subsonic crack may induce secondary intersonic cracks by using the Burridge-Andrews Mechanism or may be 'born' as intersonic. In both cases the crack circumvents the issue of having to cross the forbidden zone as a single entity.

The third point is related to the significance of the curious speed of $\sqrt{2}c_s$ that seems to repeatedly appear in many of the models discussed above. This speed is related to the energy supply (or flux) into the crack tip and has been linked to issues of favorable crack growth speeds and crack tip stability within the intersonic regime. It is also the speed at which conditions near the crack tip assume a pseudo subsonic square root singular form. Although the special significance of this speed is somehow de-emphasized by Broberg's introduction of cohesive strength (introduction of structure into the tip), this speed nevertheless persistently re-appears in relation to the laboratory and field observations to be described later. This special speed also re-appears prominently in relation to the analysis of dynamic rupture of highly dissimilar bimaterials. In this new setting, however, its physical meaning derives from issues associated with dynamic crack face contact.

The first conclusive evidence of intersonic shear crack growth in a laboratory setting was reported a few years ago by Rosakis *et al.* [32]. These experiments were designed to mimic the primary assumptions featured by all of the theoretical models described in section 2.1. Their basic purpose was to investigate whether intersonic crack growth can be observed in a highly controlled environment thus resolving, once and for all, the debate concerning the attainability of intersonic shear crack tip speeds. For this purpose, a straight-

line weak path was introduced ahead of a prefabricated notch tip in the form of a bond between two identical pieces of homogeneous isotropic material. The bonding process was carefully chosen so that the constitutive properties of the bond were very close to those of the bulk material and so that the bond width was less than $30\,\mu m$ [32]. A material system was thus constructed which, although not strictly homogeneous or monolithic, was homogeneous with regard to its linear elastic constitutive properties. However, the fracture toughness or rupture strength of the bond line was kept lower than the constituent pieces so that the material was inhomogeneous with regard to its fracture properties. The functionality of the weak bond was there to ensure the directional stability of a propagating shear crack tip, following its initiation from the asymmetrically loaded prenotch. As the issues discussed in the introduction clearly suggest, the bond is there to also mimic the theoretical assumption of a predetermined straight-line fracture path inherent in all models previously mentioned.

The geometry and relative dimensions of the specimen are shown in the insert of figure 3. Dynamic photoelasticity was chosen as a diagnostic method for capturing the stress field near the propagating fracture because of its sensitivity to maximum shear stresses. At this point it should be recalled that according to Freund's asymptotic solution [see equation (2.6)], shock waves featuring strong shear stress discontinuities are anticipated if a crack is captured to propagate intersonically. Two identical plates of Homalite-100, a brittle polyester resin that exhibits stress induced birefringence, were bonded together and the notch was machined at one edge along the bond line. In certain cases the bonding agent was polymerized *in situ* and cured appropriately to produce variable bond strengths, whereas in other cases, the bond was created by temperature-enhanced surface sintering. This later procedure does not involve any bonding agent. With such a method, there was no ambiguity regarding the constitutive homogeneity of the resulting bonded structure. The dilatational wave speed of Homalite-100 is $c_l = 2187 m/s$, the shear wave speed is $c_s = 1255 m/s$, while $c_R = 1155 m/s$. It should be noted that Homalite-100 is mildly rate sensitive and that these numbers correspond to a strain rate of $10^3 s^{-1}$. The equivalent quasistatic values for the wave speeds are approximately 15% lower. The tensile strength of bulk Homalite-100 is approximately 35MPa, while the shear strength τ_0 of the bond was approximately 14MPa.

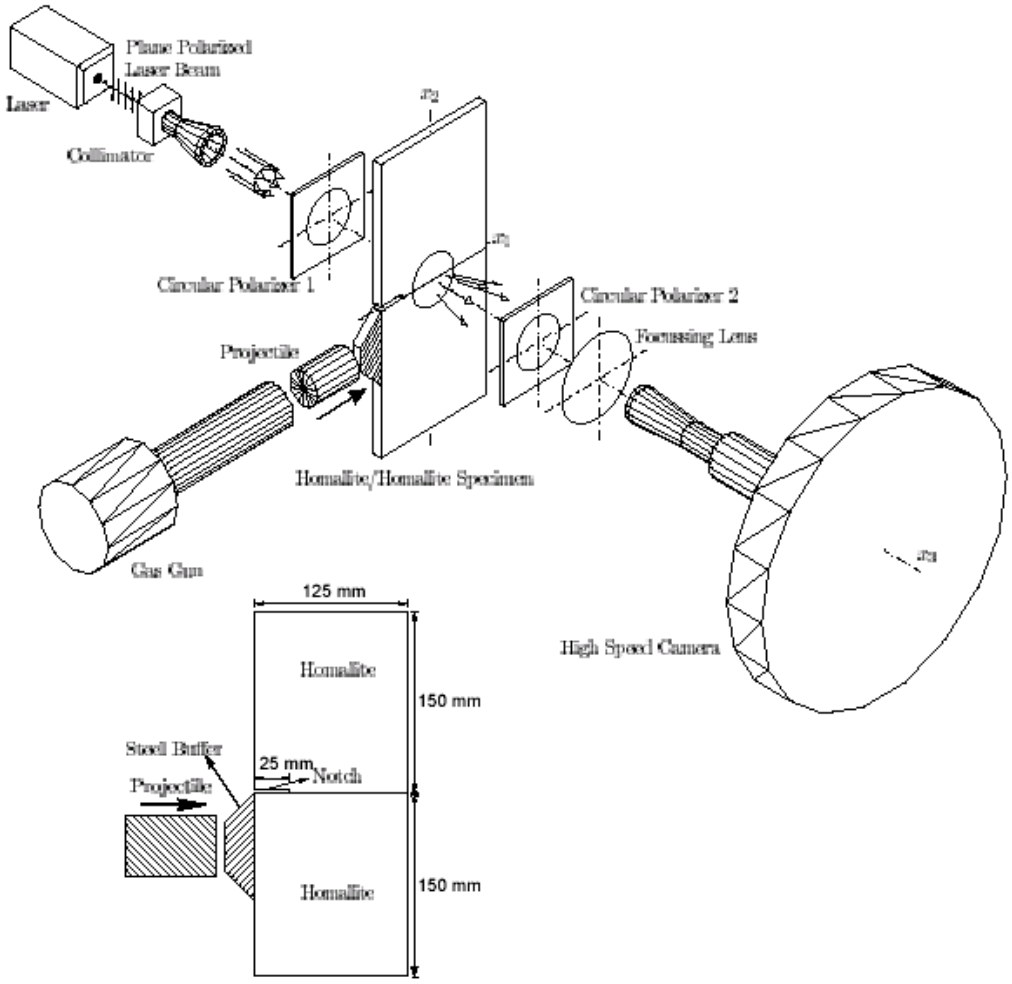

Figure 3: The dynamic photoelasticity set-up. A bonded Homalite/Homalite specimen is photographed by a high-speed camera ($2x10^6$ frames/s) as it is subjected to asymmetric impact by a projectile fired by a gas gun.

The specimen was subjected to asymmetric impact loading through a cylindrical steel projectile whose speed ranged from 8m/s to 40m/s. A steel buffer was bonded to the specimen at the impact site to prevent shattering and to induce a planar loading wave front into the Homalite plate. The compressive

longitudinal wave loads the notch which is initially in a predominantly shear mode provided that it is wide enough to prevent the transmission of stress waves into the top half. It is exactly for that reason that a notch was inserted into the specimen edge. If, instead, the specimen was directly hit below the bond line, a substantial opening component would be introduced, potentially decohering the interface in a mixed-mode fashion. The dynamic stress field produced by the impact was recorded by high-speed photography used in conjunction with a classical photoelastic set-up as shown in figure 3. The resulting high-speed sequence of photoelastic fringe patterns are contours of constant maximum in-plane shear stress τ_{max} governed by the stress optical law:

$$2\tau_{max} = \sigma_1 - \sigma_2 = nF_\sigma / h\,, \tag{2.11}$$

where F_σ is the material's stress optical coefficient, h is the specimen thickness, σ_1, σ_2 are the principal stresses and η is the isochromatic fringe order. For Homalite-100, $F_\sigma = 22.6 KN/m$.

The first experiments discussed in this article correspond to low projectile impact speeds of 20m/s. Figure 4 is a high-speed sequence of isochromatic images showing the crack initiation process. The notch is visible on the left side of the circular field of view while the prefabricated weak plane is shown as the horizontal dark line. Following the impact, the initial loading waves produce a predominately shear loading state that spreads throughout the specimen. Prior to these waves reflecting from the specimen boundaries and arriving back at the notch tip, a kinked crack is observed to initiate from the notch and to propagate along a straight-line path at approximately 70° to the weak plane. The kinked crack is a mode-I crack, which follows the path that would ensure that local crack tip deformations remain symmetric as the crack grows into the upper half of the specimen. Indeed, as discussed in section 1.1, this is an expected behaviour when a notch within a strictly homogeneous solid is subjected to pure mode-II loading. For such a case, the analysis by Hutchinson and Suo [18] predicts a kink angle of 72°, which is very close to the experimental observation. Such a result, however, is still puzzling. The solid is not strictly homogeneous since it contains a weak horizontal path that is placed there intentionally in order to capture and guide the fracture thus preventing it from kinking off to an angle. The existence of such a bond is obviously ignored by the failure sequence in this experiment and so the question remains of whether it is ever possible to propagate a shear crack under such conditions. There are three obvious ways to encourage the crack to initiate

in shear and to propagate along the bond line. The most obvious one is to intentionally decrease the bond strength even more. The second one is to impose a far-field hydrostatic stress state that would tend to discourage any mode-I opening cracks from forming. The final, and perhaps the simplest one to implement, is to increase the amplitude of the dynamically applied shear loading by simply increasing the impact speed of the projectile.

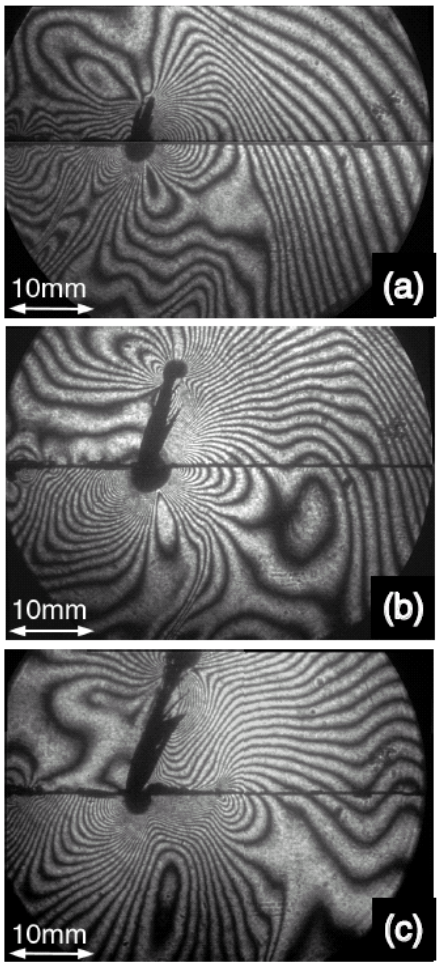

Figure 4: A sequence of isochromatic fringe patterns showing the progression of failure in a bonded Homalite/Homalite specimen subjected to low speed impact. A kinked mode-I crack is shown propagating at 72° off the horizontal weak bond.

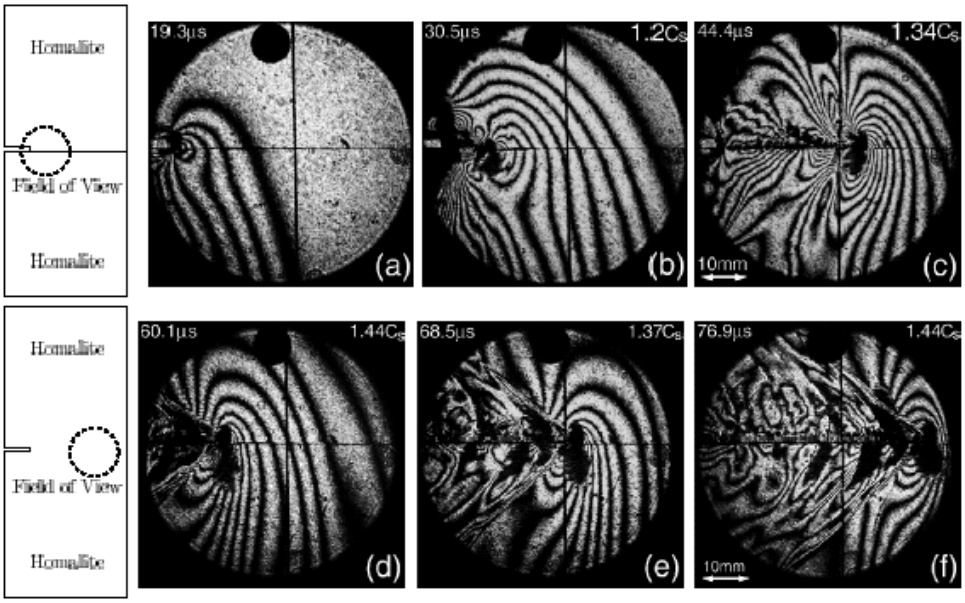

Figure 5: Isochromatic fringe pattern around a shear crack initiating from a notch and propagating along a weak plane in Homalite-100. (a-c) Field of view centered 20mm ahead of the notch tip. (d-f) Field of view centered 63mm ahead of the field of view.

Figure 5 shows what happens when the impact speed is increased from 20m/s to 27m/s, which, at first glance, seems to be a moderate change. The bond strength was left unchanged. The time elapsed after impact, as well as the crack tip speed, is shown in each frame. This selected sequence of images is drawn from two nominally identical experiments differing only by the position of the field of view. In the first three frames (a-c), the field of view of 50mm in diameter is centered on the weak plane 20mm ahead of the notch tip. In figure 5(a), the stress waves that result from the impact site and diffract around the notch tip can be observed. As they do so they simultaneously build up, at this location, the stationary stress concentration. In figure 5(b), a concentration of fringes is seen to move along the weak plane at a very high speed. This fringe concentration represents the moving shear crack tip. The next frame features a discernable increase in fringe (and thus stress) intensity around the tip and, in addition, it features the formation of visible damage trailing behind the moving

shear crack tip. The damage is confined to the upper side of the weak bond plane. In the next three frames (d-f), the field of view is centered 63mm ahead of the notch tip and, as a result, the initial notch is no longer visible. Figure 5(d) shows a crack entering the field of view from the left. The shape of the isochromatic fringes around this crack has changed, compared to its shape in the previous sequence, dramatically. In the following two frames, two lines radiating from the moving crack tip are clearly visible. These two lines are intense concentrations of fringes across which the isochromatic pattern changes abruptly and are clearly reminiscent to shock waves attached to the tips of objects moving supersonically in gases. These are clearly visible in the magnified pattern displayed in figure 6.

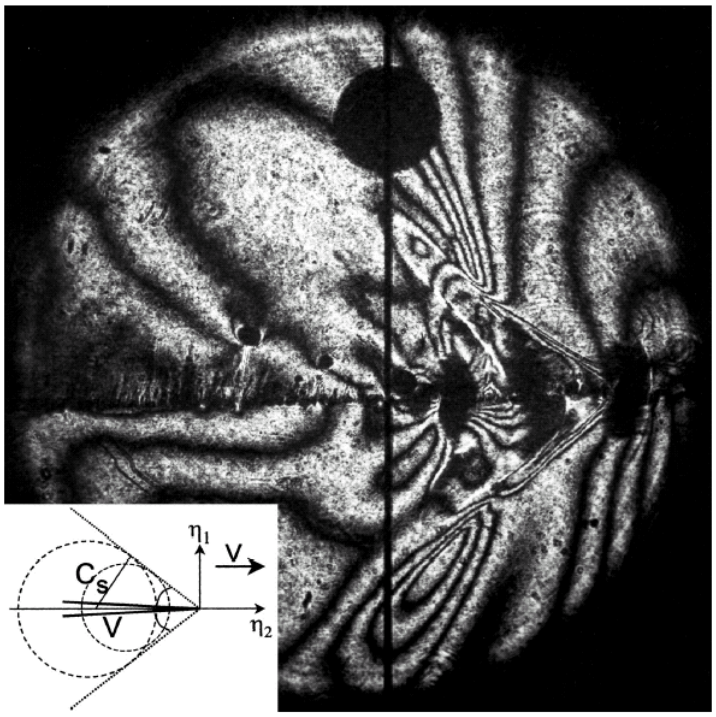

Figure 6: Enlarged view of the isochromatic fringe pattern around an intersonic shear crack moving along a weak plane in Homalite-100. A shear shock wave (Mach wave) is clearly visible.

The abrupt changes in fringe density across the two lines are clear indications of the presence of shear stress discontinuities and the two lines are two traveling shear Mach waves emanating from the crack tip as this propagates along the interface. Their existence and inclination provides clear proof that the crack tip speed has indeed exceeded the shear wave speed of Homalite-100 and is well within the intersonic regime. The angle ξ, which the Mach waves make with the crack faces, is related to the crack speed through $\xi = \sin^{-1}(c_s / v)$ and can be seen by inspection to be close to 45°. Such an angle corresponds to a crack tip speed v close to the curious speed of $\sqrt{2}c_s$ that has been extensively discussed in section 2.2. In addition, a close look at the last two frames of figure 5 reveals isochromatic fringe patterns whose similarities indicate that the propagating crack at this stage may be approaching steady-state conditions. The insights obtained by visual inspection are confirmed by more accurate analysis of the experimental results. Typical crack tip speed histories for two identical experiments varying only in the position of the field of view are shown in figure 7. The crack tip speeds are determined using two methods. The first method involves fitting a second order polynomial to every three successive points in the crack length history and then differentiating it with respect to time in order to provide the speed of the mid-point. The results are displayed in figure 7(a). In the second method, the angle of inclination of the Mach waves to the crack faces are measured and the ratio v/c_s is obtained using the Mach angle formula discussed above [i.e. $v/c_s = (\sin\xi)^{-1}$]. This method is limited to frames where the Mach waves are clearly visible. The results are displayed in figure 7(b). From figure 7(a) we see that, within experimental error, the initial crack speed is close to the shear wave speed of Homalite-100 beyond which it accelerates throughout the intersonic regime. The acceleration featured during this part of the process is of the order of $10^7 g$'s, where g is the acceleration of gravity. The maximum speed recorded is very close to the dynamic value of the dilatational wave speed of Homalite-100. After that point the crack tip decelerates gradually and ultimately reaches a steady-state speed that is slightly higher than $\sqrt{2}c_s$. This result is indeed consistent with the visual observation of Mach waves angles inclined at approximately 45° to the crack faces.

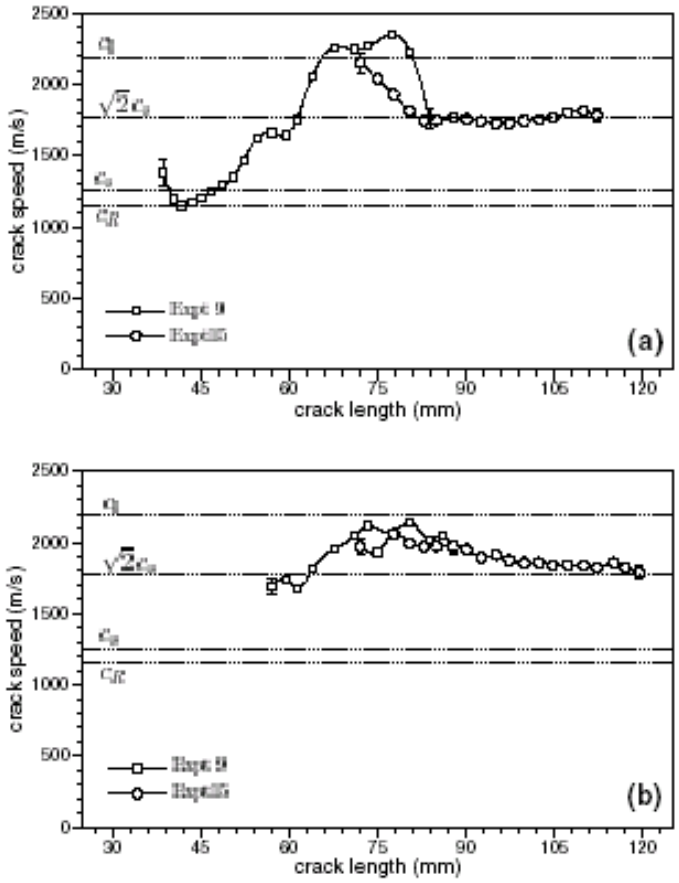

Figure 7: Shear crack tip histories. (a) Crack speed obtained by differentiation of the crack length record. (b) Crack speed inferred from Mach angle measurements.

The first experimental observations of intersonic crack propagation can now be integrated into the discussion of the early models of shear crack growth presented in section 2.1. To that effect, several points are appropriate.

The shear crack that started growing from the tip of the notch was 'born' intersonic and remained within the intersonic regime throughout our window of observation. Its ability to propagate at all speeds within this regime has provided the first unambiguous laboratory evidence that intersonic crack

growth is a physical possibility. Evidence that is consistent with the predictions of the early theoretical studies.

The crack was generated at the location of an artificially seeded singularity (stationary notch tip) whose purpose was to store energy that would induce intersonic growth. As a result, the crack was never subsonic and it never entered the forbidden crack tip speed regime between c_R and c_s. This in turn provides clear evidence of how the Burridge-Andrews Mechanism can be circumvented.

The crack tips rapid acceleration from c_s to c_l and its subsequent slow deceleration to an almost steady-state value just above $\sqrt{2}c_s$ illustrates the special significance of this particular crack tip speed. It is noteworthy that the time of this deceleration is coincidental with the arrival of the first unloading waves, which signals the disassociation of the projectile from the impact area. This is equivalent to the end of the loading pulse. It is very interesting to note that although the crack tip is largely unloaded by the arrival of this information, it still persists in propagating at a steady-state speed close to $\sqrt{2}c_s$ instead of abruptly arresting as a subsonic crack would tend to do under similar circumstances. To comprehend this behaviour one should perhaps recall that the energy supply into the tip at this particular speed is very close to its maximum. This has been pointed out in relation to Freund and Broberg's works outlined in section 2.1. The only possible discrepancy with the predictions of the cohesive theories discussed by Broberg [12] is related to the observation that the crack always tends to settle at a steady-state speed just above rather than just below $\sqrt{2}c_s$. As we will see in the following section, this discrepancy can be explained. In particular, Broberg considered the case of self-similar crack growth of a zero length crack whose two crack tips propagate symmetrically. In contrast to this model, our experimental situation involves the extension of a single crack tip that reaches as it expands nearly steady-state conditions. Therefore, a steady-state cohesive model of an intersonically moving semi-infinite crack may be much more appropriate for detailed comparisons with the experimental results.

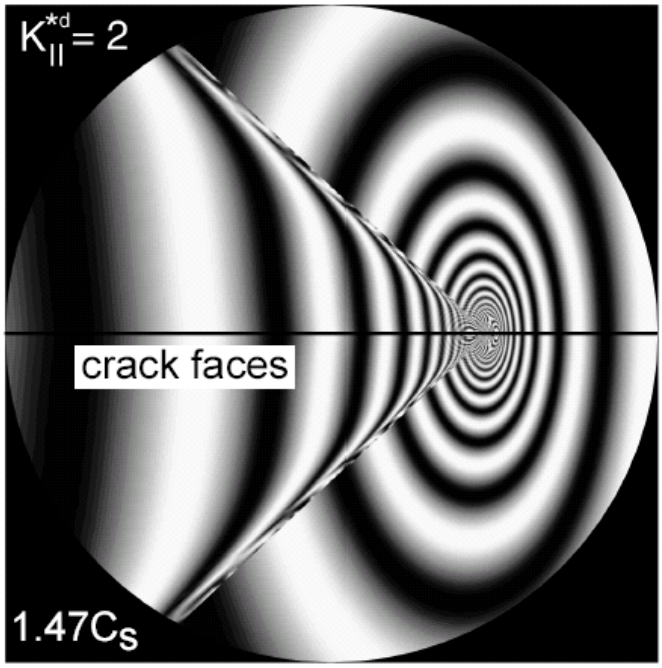

Figure 8: Synthetic isochromatic pattern constructed on the basis of Freund's 1979 singular solution [44] for an intersonically growing mode-II crack.

It is instructive to qualitatively compare the results of the experiments with the analytical predictions of Freund's [19] singular steady-state solution of an intersonically moving shear crack described in section 2.1. The comparison can be achieved when the analytical expressions for the asymptotic stress field of such a crack, given here in equation (2.6), are substituted into equation (2.11), governing photoelasticity. By using the experimental values for the fringe constant of Homalite-100, a thickness equal to that of the specimen and a best fit for the value of the intersonic stress intensity factor K_{II}^{*} ($K_{II}^{*} = 2\text{MPa m}^{q}$), a synthetic isochromatic fringe pattern is constructed. This pattern is shown in figure 8 and corresponds to a crack tip speed of $1.47c_s$. In this form, Freund's solution is directly comparable to the experimental isochromatic field shown in figure 6, which also corresponds to approximately the same speed. The two patterns are in very good agreement with respect to the prediction of the two

shear Mach waves, their inclination to the crack faces, and the overall qualitative shape of the fringes. However, ahead of the tip, the experimental fringe pattern is distorted by the stress field generated by the loading pulse. Behind the shock waves the experimental pattern is considerably more noisy than its theoretical counterpart. Possibly such a difference is due to the extensive frictional contact of the shear crack faces and the associated creation of tensile micocracks that result from this contact. Perhaps the most significant difference is in the structure of the Mach waves emitted from the tip. In the experiment, the Mach waves are not simply two sharp lines as they are in the theoretical solution. Instead, they seem to have some width and structure that is not modeled by the singular solution. This, in turn, suggests that an intersonic mode-II steady-state crack model incorporating a shear cohesive zone of finite extent, is required to model the structure of the Mach waves, as well as the crack tip process zone. The incorporation of a shear cohesive zone will also provide a mechanism for modeling the creation of tensile microdamage trailing the shear crack tip.

A closer look at the crack faces, as these appear in figure 5(c), reveals the existence of damage created on the top side of the specimen as the shear crack tip ruptures the weak bond. Figure 9(b) shows a post-mortem photograph of the upper half of the specimen in a location near the notch tip. The area in the photograph corresponds to the one enclosed by the dashed rectangle highlighted in figure 9(a). The photograph shows a series of short opening (mode-I) cracks, parallel to each other and steeply inclined to the main shear crack path. These secondary microcracks are observed all along the main crack path and are only confined to the upper half of the specimen. Their length varies from a few microns to a few millimeters. To study the statistical variation of the inclination angle of these cracks to the vertical, a number of broken specimens were assembled and inspected following each experiment. The results are shown in figure 9(c), a figure which shows the variation of crack angle with frequency of occurrence (number of secondary cracks inclined at the same angle to the vertical). It is found that the angle of inclination varies roughly from 8° to 13° with an average value of approximately 10.6°. Within the measurement error of ±1°, no strong correlation was found between the secondary crack angle and the main shear crack tip speed. The initiation, propagation, and arrest of these cracks can also be observed in real time by scrutinizing the high-speed isochromatic images at the vicinity of the crack faces.

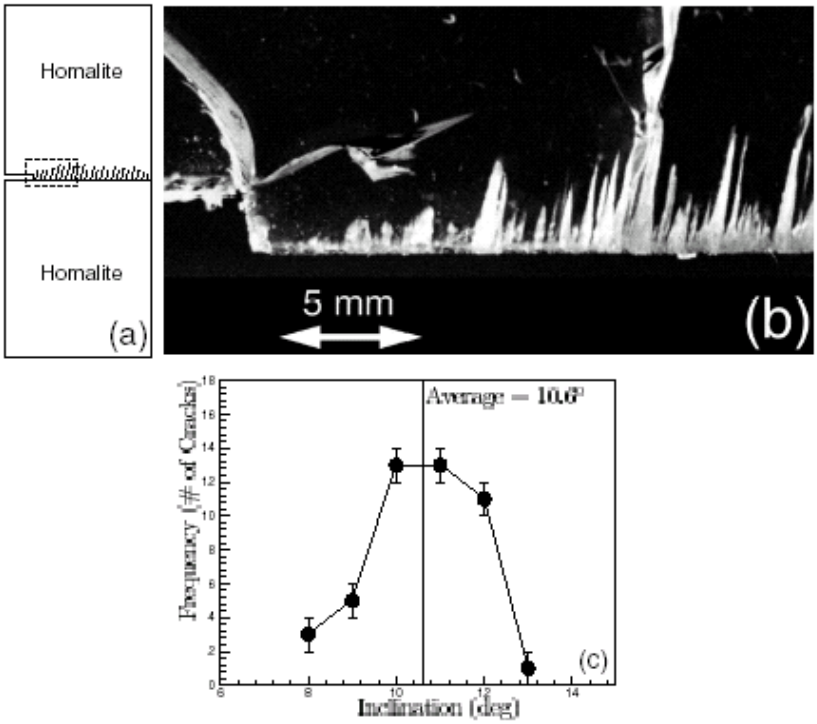

Figure 9: Mode-II microcracks formed on the tensile half of the specimen during intersonic shear rupture. (a) Schematic illustration of the specimen and the microcracks (not to scale). (b) Magnified, post- mortem view of the specimen near the rupture path. (c) Microcrack inclination angle plotted versus frequency of occurrence.

A typical photograph illustrating this phenomenon is shown is figure 10(a). A series of symmetric shadow spots mark the location of the tips of these growing mode-I microcracks as they propagate a finite distance into the upper half of the specimen. As indicated in figure 10(b), the centers of these shadow spots fall onto a straight line inclined at an angle $\alpha \sim 23°$ to the crack faces. The initial speed of these microcracks can now be estimated by: (*i*) using α , (*ii*) by using the inclination θ^* of these cracks to the vertical, and (*iii*) knowing the speed of the main shear crack. The cracks are found to be subsonic and their average speed was approximately equal to $0.6c_S$. The symmetric nature of the shadow spots is a clear indication of the tensile (mode-I) nature of the microcracks. By

extending the line passing through their tips (centers of shadow spots), it can be readily seen that these cracks nucleate at a small distance behind the main shear crack. Hence, the formation of these cracks is not akin to the typical branching phenomenon (see section 1), which involves branches or kinks emanating directly ahead of the moving crack tip. In fact, to explain the present phenomenon, the stress state just behind an intersonically moving crack at locations adjacent to the cracks faces, should be considered.

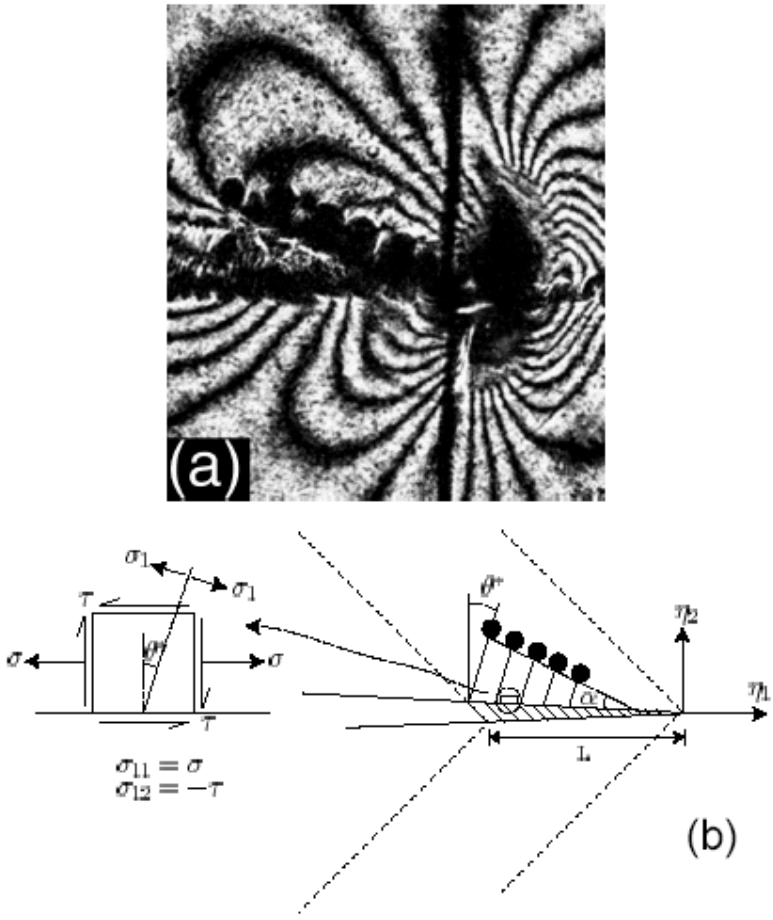

Figure 10: The mechanism of tensile microcrack formation. (a) An isochromatic image illustrating the location of the microcracks in relation to the main shear rupture. (b) An illustration of the stress state on the shear crack faces, providing an explanation of microcrack's forward inclination.

Examination of Freund's intersonic singular solution at the appropriate locations [see figure 10(b)] reveals that the direct stress σ_{ij} acting parallel to the crack faces is indeed tensile on the top half of the specimen and is compressive on the bottom. This explains why the opening microcracks are observed only in the tensile half of the specimen. However, Freund's analysis involves the assumption of traction free crack faces, an assumption inconsistent with the existence of the inclination angle that the microcracks make with the vertical. Specifically, this inclination can only be explained in terms of the presence of a more complex stress state at the immediate vicinity of the shear crack faces. As has already been seen above, it is likely that the crack faces are in contact and subsequently are undergoing frictional sliding resulting in a biaxial stress state at their initiation site. However, most of these cracks seem to originate only a couple of millimeters behind the main crack tip and in the absence of overall static normal compression. As a result, a simple way to include frictional stress at the microcrack initiation site is to introduce a shear cohesive stress zone of finite size translating with the main crack tip. Indeed, in the following section we would introduce a rate dependent line cohesive zone at the intersonic tip to explain the inclination of these secondary cracks to the vertical. Figure 10(b) shows an illustration of the cohesive region near the shear crack tip, which explains our interpretation as to the origin and directivity of the secondary tensile cracks. The main intersonic shear crack is propagating with a line cohesive zone of length L in front of it. The secondary microcracks originate on the top of the cohesive surface. The stress state at that location is two-dimensional. It features a tensile direct stress $\sigma_{11} = \sigma$ parallel to the interface, as well as a shear stress $\sigma_{12} = -\tau$ equal to the local value of the cohesive tractions resisting shear rupture $(\sigma > 0, \tau > 0)$. With such biaxial state of stress, the maximum tensile principal stress, σ_1, acts on a plane (dashed line) which is inclined at a positive angle θ^* to the vertical which is consistent with the observed orientation of the microcracks. The driving force leading to the growth of these cracks is provided by the near tip field of the intersonic crack. As the intersonic crack moves further away from the initiation site of a particular microcrack, the driving force acting on it falls. This leads to its eventual arrest a few millimeters away from the decohered shear crack faces.

2.3 The Velocity Weakening Model of Intersonic Shear Crack Propagation

In an attempt to introduce some structure into the tip of a dynamically growing shear crack, the following section discusses the results of a rate sensitive cohesive zone analysis (Samudrala *et al*., 2002).. This mode-II crack is confined to propagate steadily along a straight line simulating the weak bond between two homogeneous and isotropic half spaces. The crack propagates in the intersonic regime.

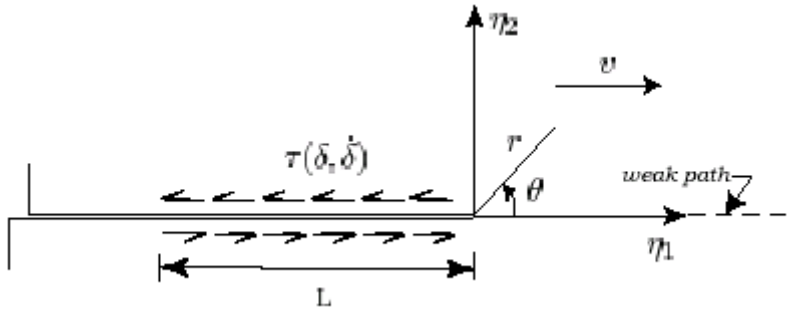

Figure 11: A schematic illustration of the shear cohesive zone and the coordinate system at the tip of the growing shear crack along a weak path.

As shown in figure 11, a shear cohesive zone of length L is located ahead of the crack tip and moves with it at an intersonic speed v. A shear cohesive zone is a line ahead of the tip within which the shear traction decays from some initial value (the initial bond strength necessary to initiate slip) to zero. The intention of this section is to show how an appropriate choice of a cohesive zone model may reconcile some of the inconsistencies observed when classical models of shear crack propagation are compared to the experiments. These inconsistencies include issues relating to the finite structure of Mach waves, the formation of secondary tensile microfractures trailing the shear crack tip, as well as issues pertaining to crack tip stability and to the identification of favorable crack tip speed regimes. Cohesive zones of the slip weakening type have been extensively used in the past to model shear ruptures [23,24,25,34]. Slip-weakening and slip-rate (or velocity) weakening models are extensions of cohesive zone models initially introduced for tensile cracks on one hand by Dugdale [35], to model plastic yielding in ductile materials, and on the other hand by Barenblatt [36] to model inter-atomic cohesion in brittle solids. A slip-weakening and a slip rate-

weakening law relates the shear strength of a cohesive surface to the local slip or to the local slip rate, respectively. Ahead of a propagating crack tip the strength decays from some relatively high peak value to zero as the physical crack tip decoheres the cohesive surface.

As was mentioned above, intersonic crack growth in our laboratory specimens was accompanied by crack face contact and sliding. Such evidence is provided by the forward inclination of the microfractures originating at the crack faces. The slip rate at this location is expected to be large, ranging from 1m/s to 10m/s. The limited data available on dynamic sliding at such high slip rates [37,38,39] also shows that the steady-state frictional stress drops with increasing slip rate. The above dynamic friction experiment motivated our use of a velocity weakening shear cohesive law. In that law, the dependence of sliding friction on local 'state' was neglected.

Rate dependent cohesive relations have been used in the past for modeling subsonic mode-I crack growth in elastic-viscoplastic material behaviour by Glennie [40] and by Freund and Lee [41]. In these studies, however, the cohesive law models a rate strengthening behaviour, which is characteristic of metallic solids. This in turn provides a very different mechanism of crack tip dissipation than the one of interest to the present study. The simple rate dependent cohesive law employed here relates the cohesive shear traction, τ , at any point within the cohesive zone to the local slip rate, $\dot{\delta}$, and is given by:

$$\tau(\dot{\delta}) = \tau_0 \left[1 + \beta \frac{\mu |\dot{\delta}|}{2\tau_0 c_S} \right], \quad \beta \le 0 . \tag{2.12}$$

In the above functional form, the parameter τ_0 represents the quasistatic cohesive strength of the weak path, $\dot{\delta}$, which is the difference between the horizontal components of the particle velocities above and below a sliding portion of the interface. The parameter, β , is a dimensionless rate parameter and is referred here as the velocity weakening parameter. β is non-positive and, as a result, the law described by equation (2.12) either represents a bond whose strength remains constant with sliding rate $(\beta = 0)$, or it represents a law whose strength decreases linearly with sliding rate $(\beta < 0)$. The form of the law in equation (2.12) is the same as the one employed by Glennie [40] and

Freund and Lee [41] in their study of subsonic mode-I crack growth. The only difference is in the sign of β which in their case was taken to be a non-negative constant. The special case of $\beta = 0$ results in a Dugdale type of cohesive zone [35].

The steady-state crack propagation problem described above is analytically tractable in the intersonic crack tip regime (Samudrala *et al*., 2002). Expressions for the stress, displacement and particle velocity fields have been obtained, but only the results that pertain to the understanding of the experimental observations presented in section 2.2 are shown here. The normalized shear stress distribution $\sigma_{12}(\eta_1)/\tau_0$ in the bond plane, $\eta_2 = 0$, is given by [33]:

$$\frac{\sigma_{12}}{\tau_0}(\eta_1 > 0) = \frac{\sin q\pi}{\pi}\left(\frac{\eta_1}{L}\right)^{1-q} * \left[\int_0^1 \frac{ds}{s^{1-q}(s+\eta_1/L)} + \int_0^1 \frac{ds}{s^q(1+s\eta_1/L)} - \left(\frac{\eta_1/L}{1+\eta_1/L}\right)^{\lambda} \int_0^1 \frac{(1-s)^{\lambda}\, ds}{s^q(1+s\eta_1/L)}\right], \tag{2.13}$$

where q is the singularity exponent for intersonic crack propagation given in equation (2.7), and λ is related to the velocity weakening parameter β and crack tip velocity v by:

$$\lambda = \frac{1}{\pi}\tan^{-1}\left(\frac{\beta v^3 \hat{\alpha}_s \sin q\pi}{c_s^3\sqrt{16\alpha_l^2\hat{\alpha}_s^2 + \left(1-\hat{\alpha}_s^2\right)^4} + \beta v^3 \hat{\alpha}_s \cos q\pi}\right). \tag{2.14}$$

The shear stress on the crack faces ($\eta_1 < -L$) vanishes. Within the cohesive zone ($-L < \eta_1 < 0$), the normalized shear stress is given by:

$$\frac{\sigma_{12}}{\tau_0}(-L < \eta_1 < 0) = 1 + \frac{\sin\lambda\pi}{\pi}\frac{(-\eta_1/L)^{1-q+\lambda}}{(1+\eta_1/L)^{\lambda}}\int_0^1 \frac{(1-s)^{\lambda}\, ds}{s^q(1+s\eta_1/L)}, \tag{2.15}$$

The normalized shear stress distribution is displayed in figure 12. Figure 12(a) shows the effect of different levels of β for a fixed intersonic speed, $v = 1.4 c_S$, while figure 12(b) represents the crack plane shear stress distribution for different intersonic speeds at a fixed $\beta = -0.4$. The choice of $\beta = -0.4$ is not random. Its significance will become clear at the end of this section. Since the horizontal distance along the bond line has been normalized by the length of the cohesive zone, the location of the tip of the cohesive zone is at the origin, while the physical crack tip lies at –1.

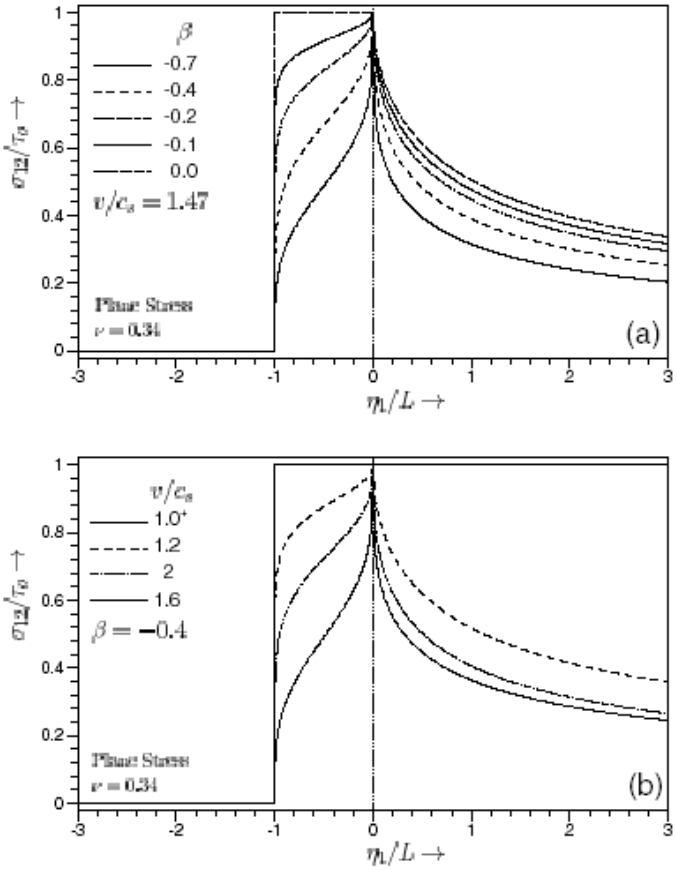

Figure 12: The spatial distribution of the shear stress σ_{12} along the rupture plane (bond line). (a) Dependence on velocity weakening parameter β. (b) Dependence on rupture speed.

Both figures have some common characteristics. As a stationary point along the bond is approached, the shear stress rises steeply and reaches the maximum value τ_0 at $\eta_1 / L = 0$. Subsequently, this particle is processed by the cohesive zone and sliding commences, the stress drops to zero at $\eta_1 / L = -1$ which is the physical crack tip. The figures show that either a lower β or a faster speed result in a faster decay of the cohesive shear tractions. Unlike Freund's singular solution, we find that σ_{12} is bounded all along the crack plane. Far ahead of the tip $(\eta_1 >> L)$, the singular solution for a sharp, structureless, crack tip is, however, recovered.

Because of mode-II anti-symmetry the values of normal stress σ_{11} just above and just below the bond line (crack line) are equal and opposite. With respect to the orientation of the experiments, the top side of the crack faces experiences a tensile σ_{11}, which is responsible for the generation of the tensile microcracks. The bottom side experiences a compressive σ_{11} of equal magnitude. The normalized stress above the crack line is given by (Samudrala *et al*., 2002):

$$\frac{\sigma_{11}}{\tau_0}(\eta_1 < -L) = \frac{\alpha_1^2 + \hat{\alpha}_s^2}{\alpha_1} \frac{sin^2\, q\pi}{\pi} \left(\frac{-\eta_1}{L}\right)^{1-q} * \left[\int_0^1 \frac{ds}{s^{1-q}(s+\eta_1/L)} + \int_0^1 \frac{ds}{s^q(1+s\eta_1/L)} - \left(\frac{\eta_1/L}{1+\eta_1/L}\right)^{\lambda} \int_0^1 \frac{(1-s)^{\lambda}\, ds}{s^q(1+s\eta_1/L)}\right] \tag{2.16}$$

on the crack line, and by:

$$\frac{\sigma_{11}}{\tau_0}(-L < \eta_1 < 0) = \frac{\alpha_1^2 + \hat{\alpha}_s^2}{\alpha_1} \frac{sin^2\, q\pi}{\pi} * \left\{\frac{\pi}{tan\, q\pi} + \left(\frac{-\eta_1}{L}\right)^{1-q} \left[PV\int_0^1 \frac{ds}{s^{1-q}(s+\eta_1/L)} + \int_0^1 \frac{ds}{s^q(1+s\eta_1/L)}\right] + sin\,\lambda\pi\, \frac{(-\eta_1/L)^{1-q+\lambda}}{(1+\eta_1/L)^{\lambda}} \left(\frac{1}{tan\, q\pi} - \frac{1}{tan\,\lambda\pi}\right) \int_0^1 \frac{(1-s)^{\lambda}\, ds}{s^q(1+s\eta_1/L)}\right\} \tag{2.17}$$

in the cohesive zone. The normal stress σ_{11} vanishes on the bond line ($\eta_1 > 0$, $\eta_2 = 0$) due to anti-symmetry. Figure 13 displays the crack plane variation of the direct-stress component, σ_{11}, acting parallel to the crack faces.

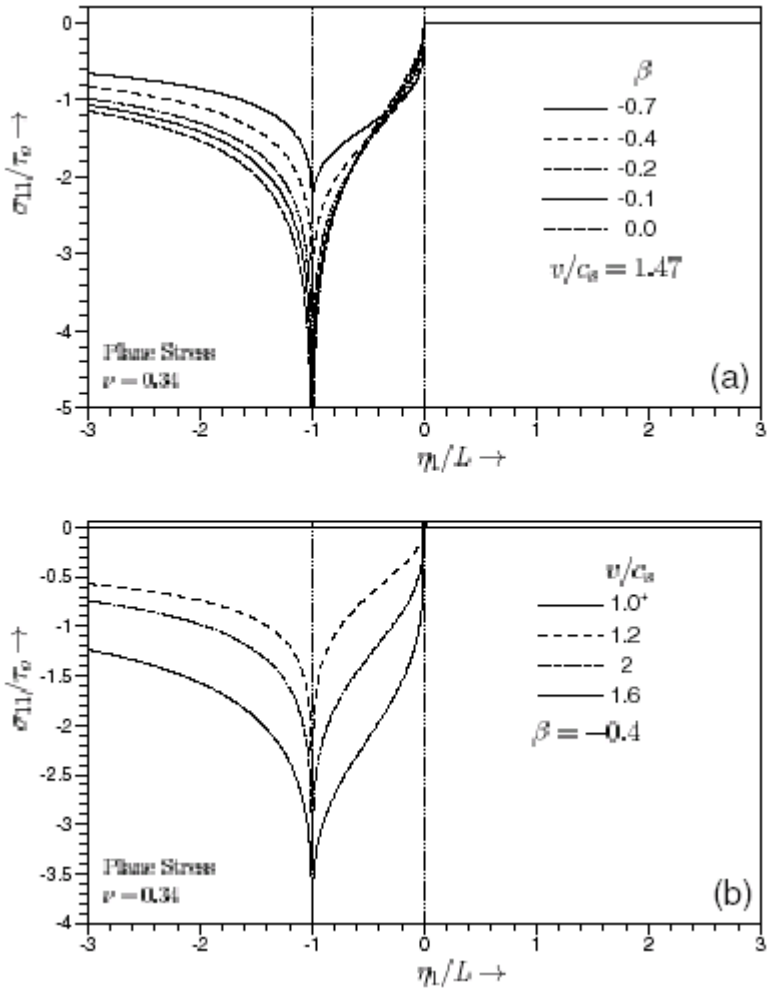

Figure 13: The spatial distribution of the direct stress σ_{11} along the rupture plane (σ_{11} acts parallel to the direction of shear crack growth). (a) Dependence on β . (b) Dependence on rupture speed.

The variation shown in figure 13 corresponds to the bottom side. The effect of β and of the speed are displayed in figure 13(a) and 13(b), respectively. In all cases, material particles above and below the bond experience zero direct stress until the arrival of the cohesive zone tip. When the cohesive zone arrives, the magnitude of the direct stresses (tensile stress above, compressive below) increases to a maximum value at $\eta_1 / L = -1$, which is the location of the physical crack tip. After this the magnitude of the horizontal direct stresses slowly decreases to zero along the newly created traction free surfaces of the crack. At this point it is worth noting that the maximum value of the direct stress is bounded for all negative values of β. On the other hand, for $\beta = 0, \sigma_{11}$ becomes singular at the physical crack tip. The value of $\beta = 0$ corresponds to the special case of a rate insensitive bond strength and a Dugdale type of cohesive zone.

Further investigation of the solution discussed above requires the determination of the cohesive zone length *L* that is expected to depend on crack tip speed, *v*, quasi-static bond strength τ_0, and some measure of the applied load. Samudrala *et al.* [33] defined a stress measure σ_{12}^D to represent the driving force of the crack. The shear stress σ_{12}^D was defined as the remote stress on the crack plane $(\eta_2 = 0)$ acting at a distance $\eta_1 = D$ ahead of the advancing crack tip. The arbitrary distance *D* should be large enough (*D* > > *L*) so that at the point along the bond the singular solution [2,19] still applies. In addition, the physical requirement that the stresses remain bounded at the front of the cohesive zone was imposed. This is a common characteristic of all cohesive zone models and in the present case results in the establishment of the following functional relationship between *L* and the parameters $\sigma_{12}^D / \tau_0, v$ and β for the entire range of intersonic crack propagation [33]:

$$L = \left(\frac{q\pi}{\sin q\pi} \right)^{1/q} D \left(\frac{\sigma_{12}^D}{\tau_0} \right)^{1/q} \left[\frac{\Gamma(\lambda - q + 1)}{\Gamma(1-q)\Gamma(1+\lambda)} \right]^{1/q}, \qquad (2.18)$$

where Γ is the standard Euler Gamma function.

The determination of L allows for the calculation of the dynamic energy release rate, G, or the energy flux into the cohesive zone per unit crack advance along the bond, per unit thickness. This is defined as:

$$G = 2\int_0^{-1} \sigma_{12}(\eta_1, \eta_2 \to 0^+) u_{1,1}(\eta_1, \eta_2 \to 0) d\eta_1. \tag{2.19}$$

In the above expression, σ_{12} and $u_{1,1}$ are the shear tractions and displacement gradients acting along the upper faces of the cohesive zone. The dynamic energy release rate G is related to the crack tip speed analytically by [33]:

$$G = \frac{\kappa + 1}{\mu} \tau_0^2 L \frac{\alpha_l^2 + \hat{\alpha}_s^2}{\beta v^3 / c_s^3} g^*(\lambda, q), \tag{2.20}$$

where $\kappa = 3 - 4\nu$ for plane strain and $\kappa = (3 - v)/(1 + v)$ for plane stress, and:

$$g^*(\lambda, q) = \frac{\lambda}{1 - q} + \frac{\sin^2 \lambda\pi}{\pi^2} \int_0^1 \frac{\xi^{2-2q+2\lambda}}{(1-\xi)^{2\lambda}} \left[\int_0^1 \frac{(1-s)^\lambda \, ds}{s^q (1 - s\xi)} \right]^2 d\xi \,. \tag{2.21}$$

The resulting variation of G with speed is displayed here in figure 14 for the intersonic regime and for only the value of $\beta = -0.4$. G is normalized by the constant G_0 which is the energy release rate associated with a quasi-statically propagating mode-II crack subjected to the same far-field load σ_{12}^D. The normalizing constant G_0 is given by:

$$G_0 = \frac{\pi(\kappa + 1)}{4} \; \frac{D\left(\sigma_{12}^D\right)^2}{\mu}. \tag{2.22}$$

As seen from figure 14, the dynamic energy release rate (energy flux into the tip) is finite throughout the intersonic regime except at speeds close to c_s and c_l. Hence, based on the requirement of a positive energy flux, the entire intersonic is admissible for mode-II crack growth. The variation of G/G_0 for intersonic speeds depends strongly on the shear strength τ_0 through the ratio

σ_{12}^{D}/τ_0. For a given value of σ_{12}^{D} as $\tau_0 \to \infty,$ the structureless singular solution [19] is recovered and the variation exhibits a well-defined finite spike centered around $v = \sqrt{2}c_s$. In most other speeds, G/G_0 is very close to zero.

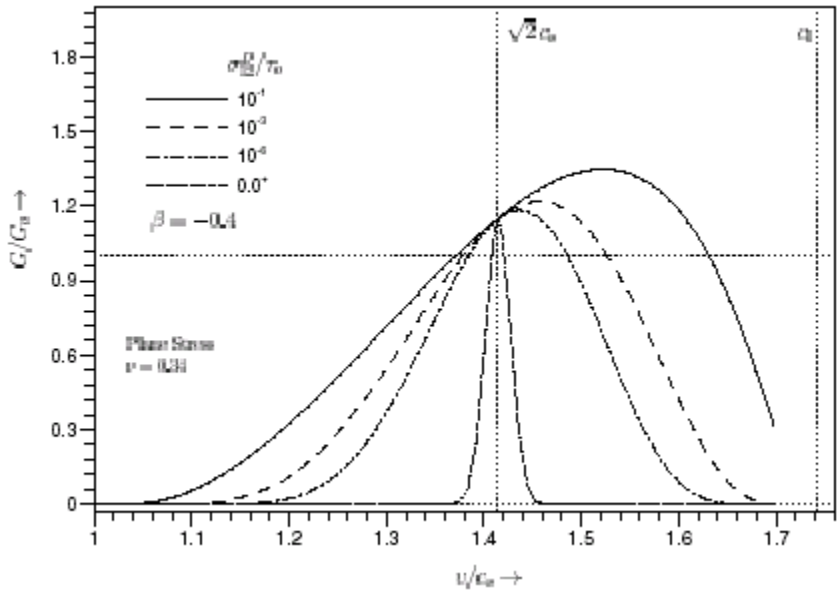

Figure 14: Normalized energy release rate as a function of intersonic rupture speed. The figure illustrates that the energy flux available to the tip has a maximum at or above $v = \sqrt{2}c_s$.

For lower shear strengths the spike becomes considerably wider and has a maximum value at speeds always higher than $\sqrt{2}c_s$. As $\tau_0 \to 0$ the peak eventually moves very close to the dilatational wave speed c_l. In the discussion of Broberg's [31] cohesive analysis, involving a self-similar expansion of a shear crack from initial zero length, the energy release rate was also found to be finite and positive throughout the intersonic regime. However, there was one important difference between his results and the results of the steady-state analysis presented in figure 14. The energy release rate G/G_0 for a self-similar crack featured a maximum, which always corresponds to a speed below rather than above $\sqrt{2}c_s$. The experiments described earlier feature speeds that approach $\sqrt{2}c_s$ from above, as the crack grows longer along the bond. This is

perhaps to be expected since the steady-state model, which involves a semi-infinite crack, becomes increasingly relevant to the experiment as the crack slowly approaches steady-state conditions (see figure 7).

Let us now turn our attention to the discussion of the tensile damage observed in the bonded Homalite/Homalite experiments. This secondary damage took the form of microcracks that nucleated at small distances (1-2mm) behind the main intersonic crack. A damage that was always confined to the upper half of the specimen. Remarkably, these cracks were all found to be almost parallel to each other with their angle of forward inclination, θ^*, varying between 8° and 13° to the normal of the weak plane. As it was argued in section 2.2. that the driving force leading to microcrack initiation is provided by the near tip field associated with the main intersonic crack. At this point, the near tip field of the velocity weakening cohesive zone model discussed above will be used in conjunction with the maximum tensile principal stress criterion in order to study the nucleation of these microcracks. Here the purpose is to determine the feasibility of secondary crack initiation and, if possible, to extract some of the unknown model parameters describing the physical system used in the experiments. The maximum principal tensile stress at any point on the upper cohesive surface is given by:

$$\sigma_1(-L<\eta_1<0,\ \eta_2\to 0^+)=\frac{\sigma_{11}}{2}+\sqrt{\left(\frac{\sigma_{11}}{2}\right)^2+\sigma_{12}^2}, \tag{2.23}$$

while the angle of inclination of the principal plane with the vertical [see figure 10(b)] is given by:

$$\theta^*(-L<\eta_1<0,\ \eta_2\to 0^+)=1/2\tan^{-1}\left(\frac{-2\sigma_{12}}{\sigma_{11}}\right). \tag{2.24}$$

For a given normalized crack speed, v/c_s, and velocity weakening factor β, the variation of σ_1/τ_0 and θ^* can be obtained within the entire cohesive zone. This is achieved by substituting the normalized stresses σ_{11}/τ_0 and σ_{12}/τ_0, which appear in figures 12 and 13, into equations (2.23) and (2.24). These variations have been analytically obtained by Samudrala *et al*. [33] and will not be shown here. In assuming that the material obeys the maximum principal stress criterion for brittle fracture, a tensile microcrack would initiate at a point $\eta_1=-L^*$ in the upper cohesive surface where the tensile principal stress reaches

a critical level σ_u (i.e. $\sigma_1 = \sigma_u$). This critical stress level σ_u is the ultimate tensile strength of the homogeneous material, which for monolithic Homalite is equal to 35MPa. The location L^*, where this criterion is first satisfied, corresponds to a particular value of the principal angle θ^*.

By using the procedure elaborated by Samudrala *et al*. [33], the functional dependence of θ^* on $v/c_s, \sigma_u/\tau_0$, and on β can be obtained. For a particular material system and bond strength σ_u/τ_0 is fixed and can be measured in the laboratory. For the experiments discussed above, this ratio is equal to 2.5, but the value of β, the velocity weakening parameter, is much more elusive. This is due to the scarcity of experimental information available in the literature on dynamic sliding. In fact, the nature of the velocity weakening behaviour experienced within the cohesive zone is unknown. To provide a realistic first order estimate of β, the angle of inclination θ^* of the microcracks is plotted in figure 15 as a function of β. The effect of different intersonic speeds is also displayed. The ratio σ_u/τ_0 is taken to be equal to 2.5.

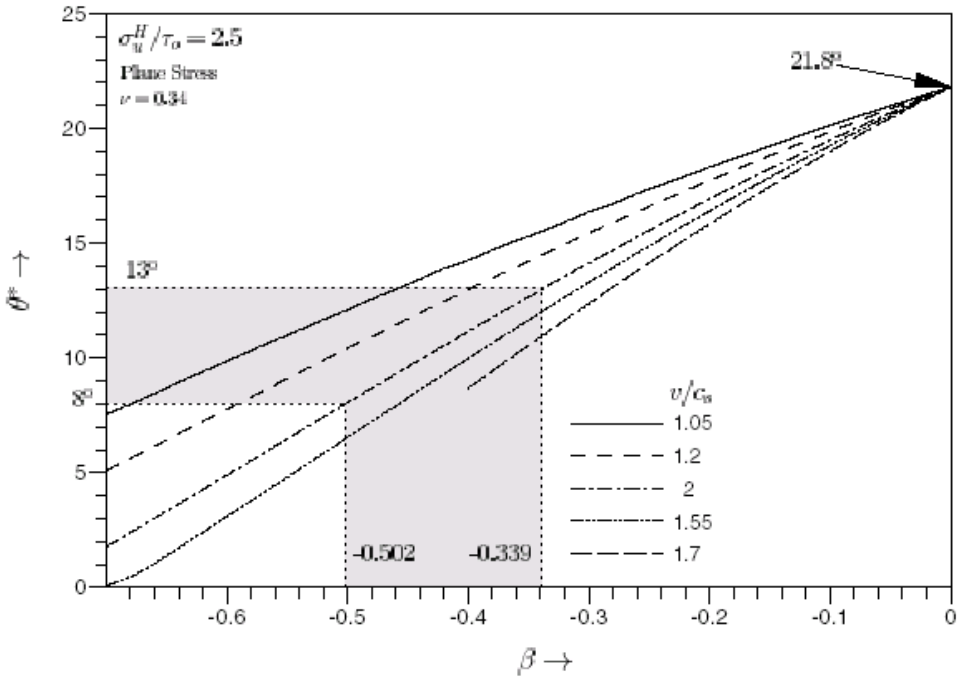

Figure 15: Inclination angle of microcracks to the vertical, plotted as a function of the slip rate weakening parameter β.

The figure shows that a maximum angle of inclination of 21.8° is obtained for the rate insensitive case of $\beta = 0$ (Dugdale zone). For this case, the angle is independent of crack tip speed. As β decreases θ^* is monotonically reduced. For example, for $v = \sqrt{2}c_s$, the inclination reaches the experimentally observed average value of 11° at $\beta = -0.4$. However, at this value of β, the angle of inclination varies with the intersonic speed, from approximately 8° to 14.5°. The predicted variation is very close to the statistical variation reported in figure 9(c). Therefore $\beta = -0.4$ is an optimal estimate for the conditions that prevail in the Homalite/Homalite experiments.

Having established the optimal value of the velocity weakening parameter β, the cohesive zone solution can be used to construct 'synthetic' isochromatic patterns. A direct visual comparison of the model with the experiment is now possible. Figure 16 shows two such synthetic photoelasticity patterns corresponding to two intersonic crack tip speeds and to identical material properties. The details leading to their construction can be found in Samudrala *et al*. [33]. In both figures, we can see that the presence of a cohesive zone gives a finite width to the Mach waves and it reveals the existence of a distinctive fringe structure. Such a structure is shown magnified on the right part of each figure. In figure 16(a), the crack tip speed is equal to $1.2c_s$ and the cohesive zone size is 5mm. In figure 16(b), the crack tip speed is equal to $1.6c_s$ and the cohesive zone size has dropped to almost 2.6mm. The inclination of the Mach waves, as well as the shapes of the isochromatic fringes behind the Mach lines, are noticeably different.

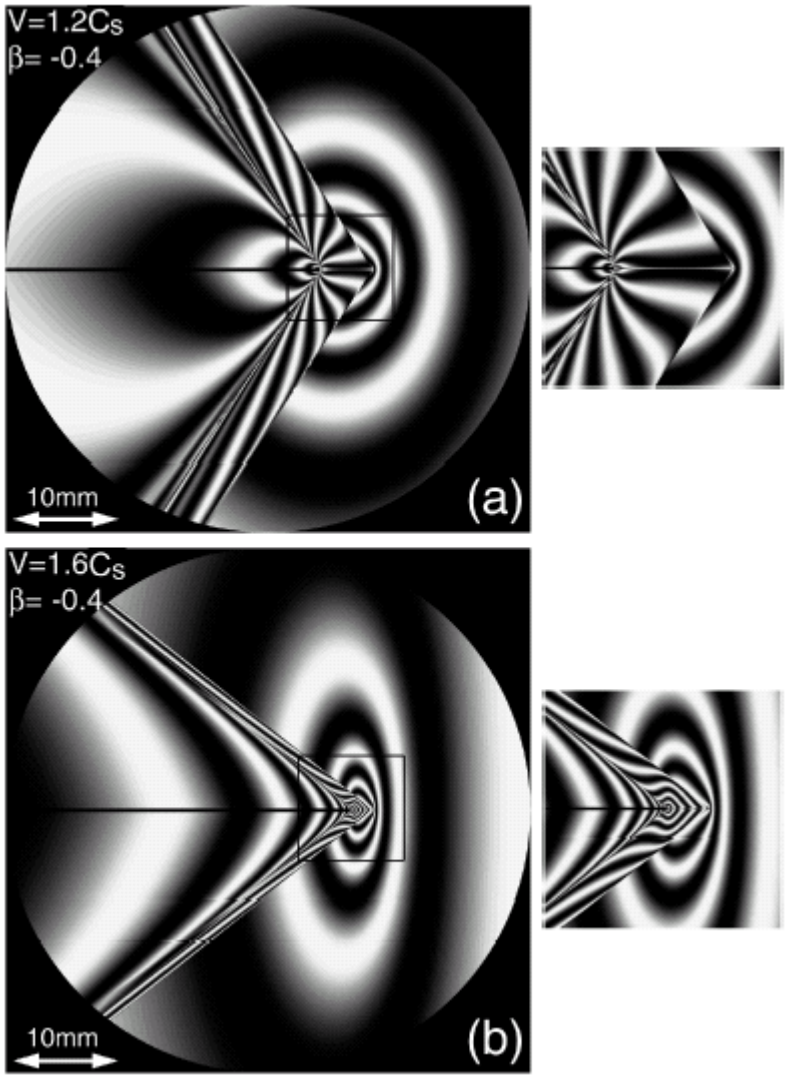

Figure 16: Synthetic isochromatic patterns constructed using the steady state velocity weakening cohesive zone model of Samudrala *et al*. (2002).

2.4 Recent Continuum and Atomistic Models of Intersonic Shear Crack Propagation

We conclude our discussion of intersonic shear crack propagation of bonded identical isotropic solids by briefly reviewing some recent important analytical and numerical contributions of significance to the dynamic fracture literature. Using a newly developed cohesive element methodology in conjunction with the finite element method, Needleman [42] simulated the Homalite/Homalite experiments described earlier. He conducted a highly systematic study of the parameter space of relevance to the intersonic crack propagation. In particular, his work examined the effect of shear strength, of fracture energy, and of projectile impulse duration on the subRayleigh to intersonic transition. If the projectile pulse duration is not cut off, the shear crack propagates at c_R provided the bond strength remains high enough to prevent intersonic growth. If the bond strength is lowered, the crack, after spending some limited time at c_R, accelerates to a constant intersonic speed above $\sqrt{2}c_S$. As the bond strength becomes even weaker, the crack tip speed approaches the dilatational wave speed of the solid. The transition from Rayleigh to intersonic speed is found to involve the Burridge-Andrews Mechanism. When the duration of the pulse is cut off, the intersonic crack decelerates to $\sqrt{2}c_S$ and after a while it becomes subRayleigh and it then abruptly arrests. Needleman's numerical work has been crucial to our understanding of the intersonic shear crack propagation.

Using a spectral boundary element method, Geubelle and Kubair [43] studied the problem of transient initiation and growth of a mixed-mode crack propagating along a straight-line path under the axiom of asymmetric far-field loading. Their work employs the use of quasi-linear rate independent cohesive failure model, which couples the normal and the shear cohesive failure modes. Their work examines the loading and bond strength conditions under which mode-II and mixed-mode crack growth can occur in either the subRayleigh or the intersonic speed regimes. For the purely mode-II case and for the low values of bond toughness, their results show that subRayleigh crack propagation is possible only for moderate values of the shear loading. For higher values of bond toughness no subRayleigh regime is observed and what is only possible is intersonic growth.

For the mixed-mode case, Geubelle and Kubair [43] found that the higher the shear component of the applied load the lower the load level required to achieve intersonic crack propagation. For subRayleigh mixed-mode crack growth both opening and sliding displacements are observed at the cohesive zone. However, for intersonic crack growth only sliding displacements appear near the growing tip and opening displacements appear only outside the cohesive zone. This is a remarkable observation since it links local shear failure to intersonic conditions even when the far-field loading is not purely asymmetric.

Abraham and Gao [44] performed the first atomistic simulation of shear crack propagation along a weak interface. This interface was between two harmonic crystals and characterized by a Lennard-Jones potential. Their simulations showed that a shear dominated crack, or atomistic rupture, accelerates to c_R soon after initiation. At that point, the crack promotes the nucleation of an intersonic microcrack that travels at c_l, in accordance with the Burridge-Andrews Mechanism.

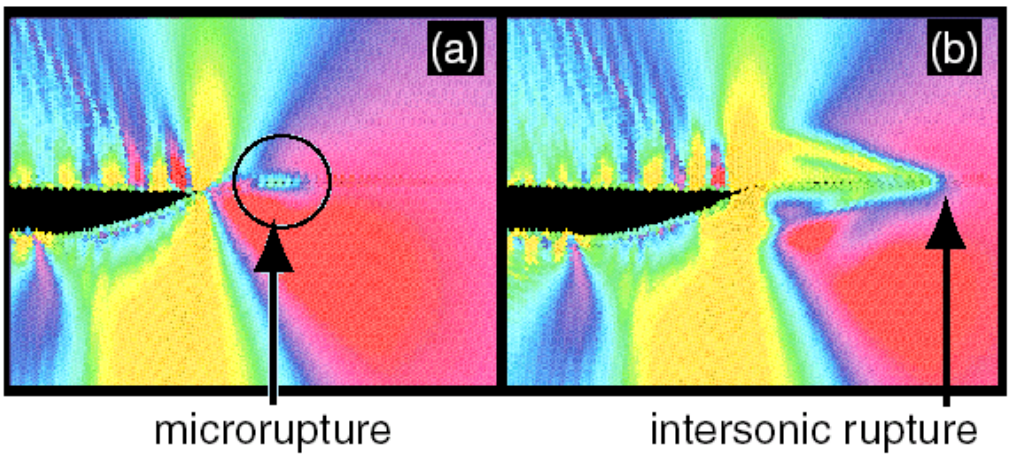

Figure 17: The first atomistic view of the 'Burridge-Andrews Mechanism' responsible for subRayleigh to supershear transition (Abraham and Gao, 2000).

A visual demonstration of the nucleation of the secondary microcrack in front of the primary Rayleigh crack has been illustrated by Abraham and Gao

[44] and is displayed in figure 17. Figure 17(a) shows the primary crack and it also illustrates in front of it, along the bond, a small decohered line, which is indicated by an arrow. Initially, the microcrack propagates at approximately the shear wave speed. Shortly thereafter, the two cracks join up and the combination accelerates through the intersonic regime as it is evidenced by the two inclined Mach waves attached to the tip. When the simulation involves bonded harmonic crystals, which mimic the linear elastic behaviour, the recorded terminal speed is c_l. When the applied far-field strains are subsequently relaxed, the crack decelerates to $\sqrt{2}c_s$ in a manner similar to the one observed in the Homalite/Homalite experiments of section 2.2.

The possibility of supersonic crack growth was investigated by Abraham and Gao [44] and recently by Abraham [45] in a three-dimensional simulation involving bonded unharmonic crystals. In this study the local wave speeds at the highly strained crack tip region are higher than those of the unstrained bulk solid. This is due to the nature of the specific unharmonic potential used in the study. Consequently, the crack is able to propagate supersonically with respect to the 'linearized' wave speeds (unstrained limit) of the crystal. However, with respect to the wave speeds of the highly strained crack tip region, the crack is still p-sonic.

The clear observation of the subRayleigh to intersonic transition, as well as the reappearance of the curious speed of $\sqrt{2}c_s$ in an atomistic setting, is extremely significant. Indeed, the scale at which the atomistic calculation is performed is six orders of magnitude smaller than the laboratory experiments. Yet, the main features observed under laboratory situations and those predicted by continuum theory, are still preserved to a remarkable level of detail. To demonstrate that point conclusively, Gao *et al.* [46] compared the atomistic calculations with continuum level analysis thus demonstrating the magnificent predictive power of continuum mechanics over a variety of length scales. Without any parameter fitting, the continuum analysis agrees very well with molecular dynamics simulations.

Finally, the most recent analytical contributions to the subject of intersonic crack growth include the work by Huang and Gao [47] and by Antipov and Willis [48]. Huang and Gao [47] obtained the fundamental solution of a transient intersonic mode-II crack propagating in an elastic solid as well as the associated cohesive zone solution. A stationary crack is subjected to a pair of

shear forces τ^* at the crack tip, and the crack tip begins to propagate with an intersonic crack tip velocity ($v > c_s$) at time t=0. The shear stress ahead of the intersonic crack tip is given by:

$$\sigma_{12}(\eta_1 \to 0+) = f(v)\frac{\tau^*}{vt}\left[\frac{\left(v^2 - c_s^2\right)t}{(c_l + v)\eta_1}\right]^q, \qquad (2.25)$$

where $f(v)$ is a non-dimensional function of the crack tip velocity, and q is the exponent of stress singularity given in equation (2.7). This fundamental solution provides the general solution for an intersonic shear crack subjected to an arbitrary initial equilibrium field. Antipov and Willis [48] obtained the fundamental solution for an intersonic crack propagating in a viscoelastic solid. Huang and Gao [49] further studied the arrest of an intersonic crack tip, and obtained the transient solution for a suddenly arrested intersonic crack after such crack has propagated for a finite time t^* The arrested crack tip resumes the square root singularity, but the stress intensity factor does not instantaneously reach its equilibrium value, or the value expected, for a stationary crack tip subjected to the same loading. This is contrary to a suddenly arrested subRayleigh crack, for which the stress intensity factor *immediately* reaches the static value after being arrested [see equation (2.3)]. An arrested intersonic crack tip is unable to reach the equilibrium field instantaneously because the Rayleigh and shear waves are still trailing behind it. Figure 18 shows the normalized stress intensity factor, $K/K_{equilibrium}$, versus the normalized time, t/t^*, for the arrested intersonic crack tip, where $K_{equilibrium}$ is the equilibrium value of K (i.e., $t \to \infty$), and the intersonic crack tip velocity just before arrest is v=1.1c_s. A vertex in the figure is observed, corresponding to the arrival of the shear wave (t=vt^*/c_s) at the arrested tip. Immediately after the Rayleigh wave arrives at the tip (t=vt^*/c_R), the stress intensity factor reaches its equilibrium value $K_{equilibrium}$. This indicates that the arrested intersonic crack tip reaches its equilibrium value for a static crack tip after a finite time delay which is just enough for all waves to catch up. Gao et al. [51] studied both suddenly accelerating and decelerating intersonic shear cracks and established that, for intersonic cracks that decelerate to subRayleigh speeds, the stress intensity factor in equation (2.3) is reached only after all the Rayleigh and shear waves

catch up with the subRayleigh crack tip. For an intersonic crack that accelerates or decelerates to another intersonic crack tip speed, equation (2.3) never holds because the trailing Rayleigh and shear waves can never catch up.

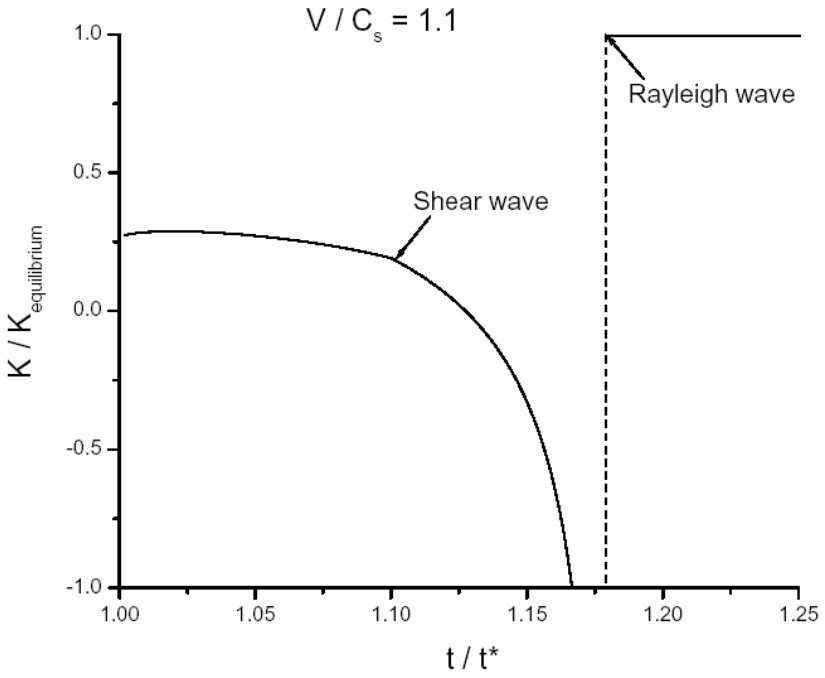

Figure 18: The normalized stress intensity factor, $K/K_{equilibrium}$, around a suddenly arrested intersonic crack tip, $K_{equilibrium}$ is the equilibrium value of the stress intensity factor (i.e., time $t \to \infty$), time t is normalized by the crack propagation time t^*, Poisson's ratio = 1/3, the crack tip velocity is v=1.1c_s, and c_s is the shear wave speed.

3. CRACK PROPAGATION IN WEAK PLANES BETWEEN TWO CONSTITUTIVELY HOMOGENEOUS, ANISOTROPIC SOLIDS

Our discussion so far has concentrated on constitutively homogeneous and isotropic solids that contain weak paths along which shear cracks may be trapped and may propagate dynamically. We have demonstrated that such shear

cracks may attain intersonic speeds and may propagate as fast as the dilatational wave speed of the isotropic material. We have investigated issues of crack tip stability and have shown that certain multiples of the isotropic wave speeds delineate the boundaries of acceptability of stable intersonic shear crack propagation. In this section, we extend our discussion to the study of dynamic cracks in simple anisotropic materials also containing preferable crack propagation paths. In particular, we will discuss recent experiments by Coker and Rosakis [52], who studied dynamic crack propagation in thick unidirectional fiber reinforced composite plates subjected to impact loading.

Dynamic crack growth along weak planes is a predominant mode of failure in all types of structural composite materials, as well as in most layered graded or sandwich structures. With increasing demand for specialized, lightweight, and high-strength structures, the failure mechanisms encountered in such composites have been receiving increased attention from the engineering community. The particular case of a unidirectional graphite fiber, polymer matrix, composite that will be discussed here represents perhaps the simplest case of a truly anisotropic material of some practical significance. When viewed 'macroscopically', the details of the fiber dimension and local properties become invisible and a homogenized constitutive description may be adopted. Through this homogenization, the composite material appears as 'anisotropic' but is still considered constitutively homogeneous and features drastically different stiffness and wave speed along different directions. In addition to introducing wave speed anisotropy, the fibers also have another effect. They also feature weak crack paths along their interface with the matrix. These paths are lines along which the fracture resistance of the solid is drastically lower than any other direction. As a result, the solid can be viewed as inhomogeneous regarding its resistance to fracture in much the same way the bonded Homalite/Homalite plates were viewed earlier.

Figure 19 shows the geometry of the composite plates used in the fracture experiments. It also displays micrographs of the fiber microstructure corresponding to two areas within the plate thickness. Unidirectional composites of the type shown in figure 19 are modeled by a very simple anisotropic constitutive law and are known as 'transversely isotropic' materials. The details of their constitutive description are given by Coker and Rosakis [52] together with the values of various physical properties of the particular material under consideration. The particular type of material anisotropy introduced by the fibers results in different bulk wave speeds of dilatational waves traveling along the two principal directions of anisotropy.

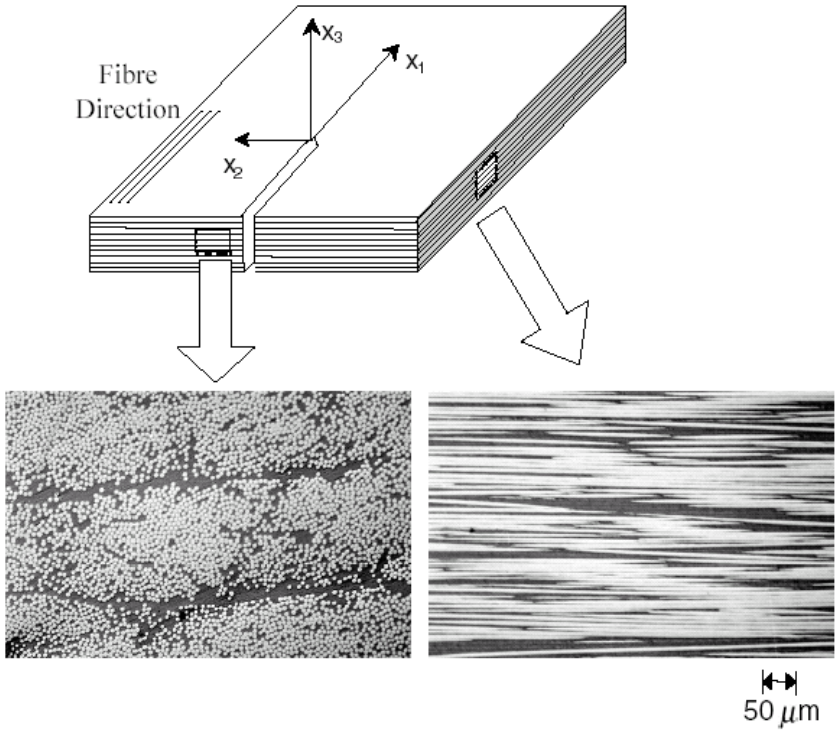

Figure 19: View of a thick composite plate containing a notch. The micrographs provide cross-sectional views of the microstructure of the unidirectional graphite-epoxy material.

The shear wave speed, however, is independent of direction. The dilatational wave speed along the direction of the fibers, c_l^{II}, is equal to 7500m/s, the dilatational speed perpendicular to the fibers, $c_l^{\perp}$, is equal to 2700m/s while the shear wave speed, c_S, is equal to 1550m/s. It should be noted that $c_l^{\perp}$ is only slightly higher than that of the polymer matrix, while c_l^{II} is slightly lower than that of the graphite fibers. Also, $c_l^{II} = 2.8c_l^{\perp}$. The Rayleigh speed c_R^{II} of surface waves propagating parallel to the fibers on the surface of a transversely isotropic half space of the same material considered by Coker and Rosakis [52]

is $c_R^{II} = 0.99c_S = 1548$ m/s. Plates of the type shown in figure 19 were subjected to impact loading through a projectile fired by a gas gun at speed varying from 10m/s to 57m/s. A schematic diagram of the experimental arrangement is shown in figure 20.

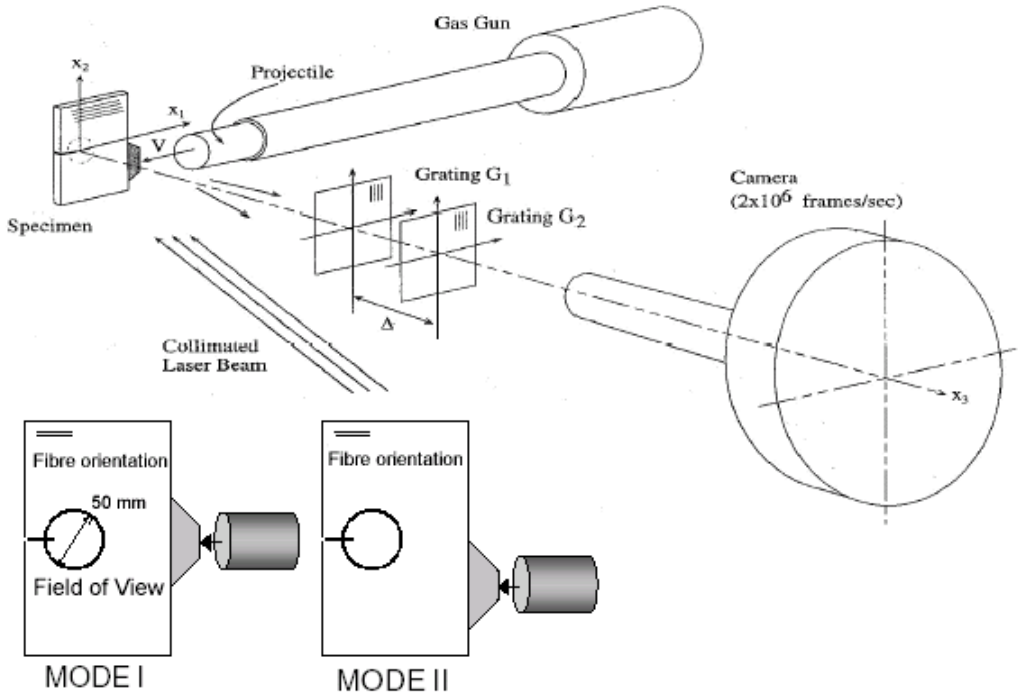

Figure 20: Diagram of the high-speed photography experimental set-up and the optical method of CGS shown in a reflection arrangement.

The plates were impacted at the plate's edge opposite the initial notch. When the projectile impacted the plate along the specimen center line, the resulting stress waves loaded the initial notch symmetrically and the resulting failure was in the form of a growing mode-I crack. When the specimen was hit below the center line, the loading of the notch was shear dominated and the resulting failure proceeded in the form of a mode-II crack. In both cases, the existence of weak fiber/matrix interfaces force the crack to grow directly ahead of the notch tip along the horizontal center line. In order to record the history of crack

growth, the method of Coherent Gradient Sensing, CGS [11], was used in a reflection arrangement and in conjunction with high-speed photography ($2x10^6$ frames/s). The fringe patterns visible in the images that follow are contours of equal out-of-plane surface displacement gradient, $\partial u_3 / \partial x_1$. They are intimately related to the stress state near the propagating crack tip and their shape and size reflects the nature and the intensity of the near tip singularity.

3.1 Symmetric Crack Growth along the Fibers

Symmetric, mode-I, crack tip deformations were obtained by impacting the specimen symmetrically along the notch line as described earlier. Four images from a sequence of CGS interferograms, corresponding to mode-I crack initiation and growth, are shown in figure 21 for the highest impact speed of 57m/s. Images of this type allow for the measurement of crack tip speed and for the estimation of dynamic fracture parameters.

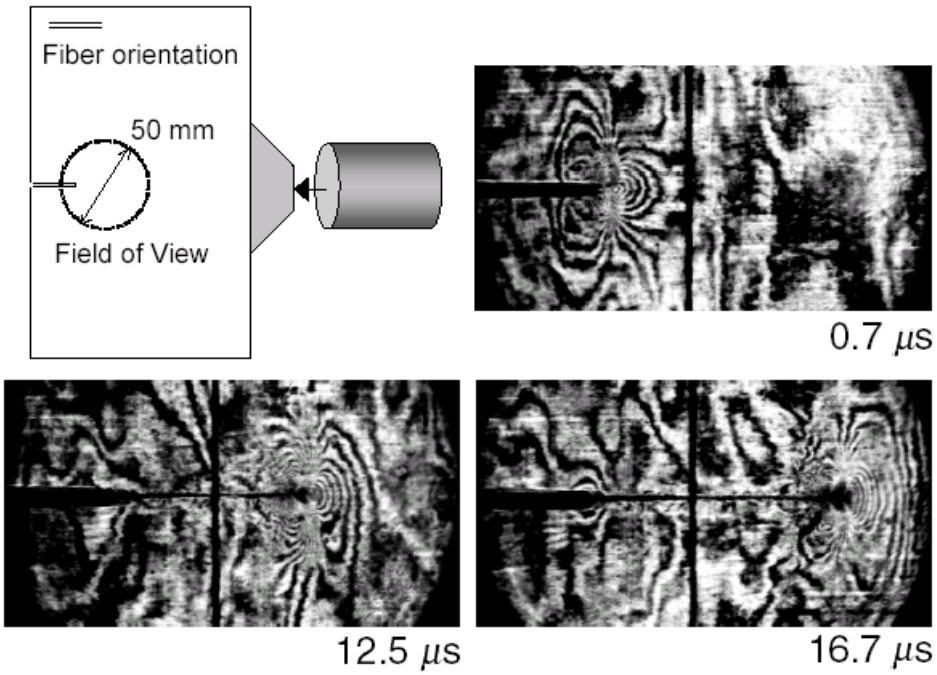

Figure 21: CGS interferograms illustrating the process of initiation (from a notch) and dynamic growth (along the horizontal fibers) of a mode-I crack in a unidirectional composite plate.

The images show that for the symmetric loading case, the resulting mode-I cracks propagate dynamically along the fibers, ahead of the initial notch tip, and attain very high speeds without displaying any tendency to branch. The crack tip speed histories of three mode-I experiments corresponding to three different projectile impact speeds are shown in figure 22. As the impact speed is gradually increased so is the speed of the resulting mode-I cracks. However, there is a critical level of impact speed beyond which changes in crack tip speed are no longer achievable. In fact, as it is discussed by Huang *et al*. [53] and Coker and Rosakis [52], the mode-I cracks seem unable to ever exceed the Rayleigh wave speed of the composite (horizontal line) irrespectively of the far-field energy available to it through impact loading. This phenomenon is very consistent with the discussion presented in section 1.2. It is analogous to the behaviour of dynamic mode-I cracks in bonded isotropic solids and shows that c_R^{II} is still the limiting speed of the transversely isotropic solid in the presence of preferable crack paths along the fibers.

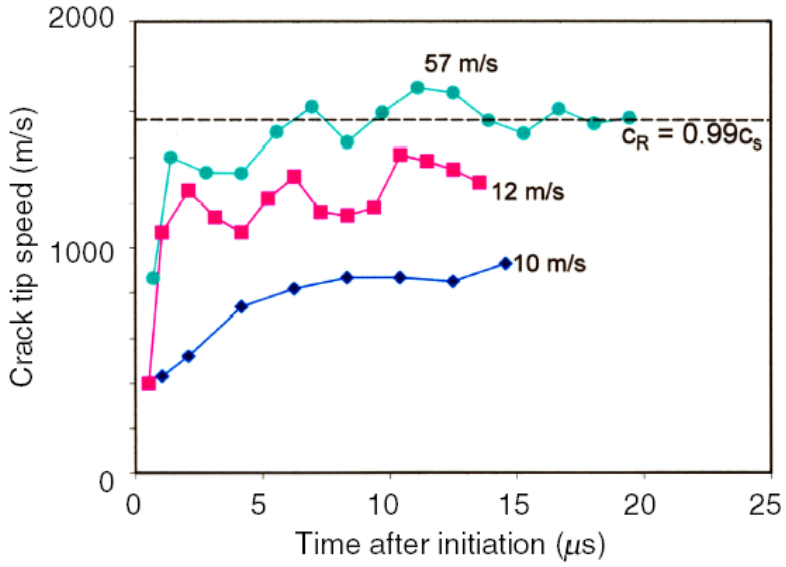

Figure 22: Mode-I crack tip speed histories. As the impact speed increases the crack tip speed reaches, but never exceeds, c_R.

3.2 Shear Crack Growth along the Fibers

In the asymmetrically loaded experiments, the impact wave compression propagates from one end of the plate to the other (side of the notch) and, just below the notch, is being reflected as a tensile wave. This reflection loads the notch in a predominately shear mode inducing dynamic shear rupture. Figure 23 is a sequence of four CGS interferograms and it illustrates the crack initiation and shear crack growth process. Figure 23(a) shows the mode-II fringe pattern that has developed around the notch as it is loaded by the arriving wave. As the crack initiates and grows along the straight-line fibers, the nature of this fringe pattern changes significantly. The fringes are pulled back and are elongated. The rounded fringe loops change to a triangular wedge, which is bounded by lines of high concentrated fringes emerging from the crack tip at a well-defined angle. Eventually these lines broaden into more parallel line structures [see figures 23(c) and (d)], which intercept the crack faces a few millimeters behind the propagating crack front.

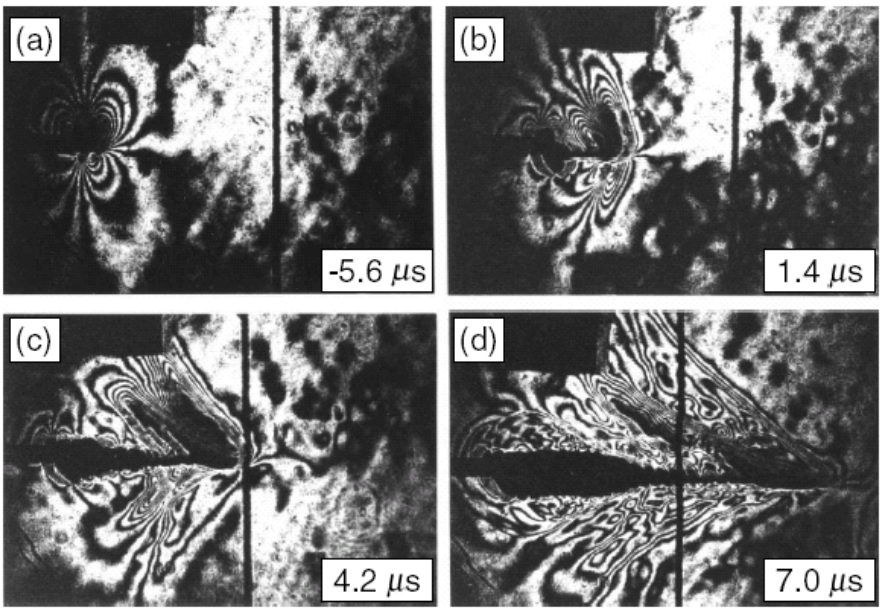

Figure 23: A shear rupture propagating intersonically along the fibers of a unidirectional composite plate. The high-speed images are obtained in a reflection arrangement through CGS interferometry. Fringe patterns correspond to contours of surface slope component along the horizontal.

The observed structures are indeed reminiscent of the isochromatic images presented earlier in figures 5 and 6 in relation to intersonic crack growth in bonded isotropic Homalite/Homalite plates. A major difference, however, is that the images presented in figure 23(c) are specularely obtained by reflection of light from the specularely reflective surface of the composite plate. Also, the absolute magnitude of the maximum observed crack tip speed is unprecedented and approached 7500m/s, which is approximately 3.4 times higher than those observed during intersonic shear rupture of the Homalite/Homalite system. Finally, one should note that the clear formation of double shock waves, visible in the photographs, provide clear evidence that dynamic large-scale frictional contact takes place on a scale much higher than in the Homalite/Homalite system.

Figure 24 collectively displays the speed histories of three different shear (mode-II) crack growth experiments. For comparison purposes, the speed history of the fastest recorded mode-I crack in the same material system is also shown.

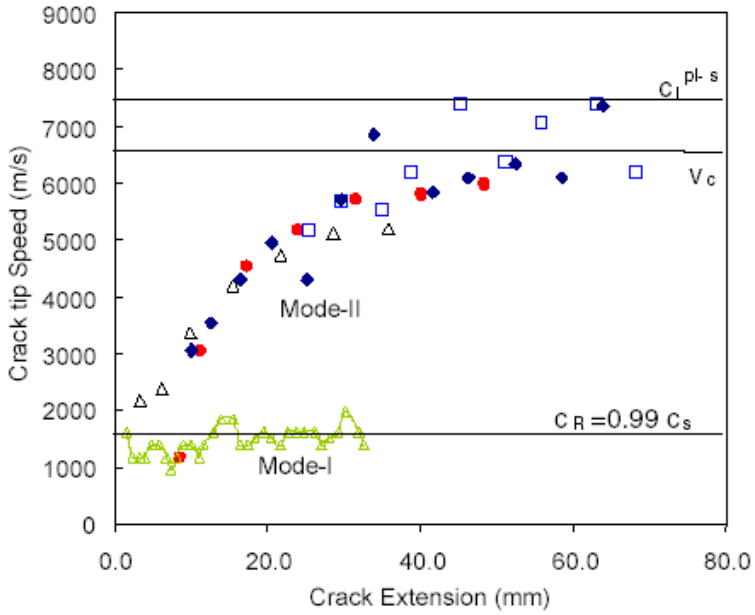

Figure 24: Mode-II rupture speeds as a function of crack tip position. The speed history of a mode-I crack in the same composite material is also shown for comparison. Maximum speeds as high as 7.5 km/s were recorded.

The general trends for the shear dominated crack growth is to initiate within the intersonic regime, to accelerate up to 7500m/s, which is the dilatational wave speed along the fibers, and to then oscillate between this speed and another speed, v_c. The speed v_c is well defined in the experiments and is equal to 6500m/s. This phenomenon is highly repeatable and suggests that v_c may have some special significance worth of theoretical scrutiny. How exaggerated and unprecedented this maximum mode-II crack tip speed really is can only be appreciated by comparison to the mode-I case. As shown in the bottom of figure 24, the classical mode-I opening cracks never exceed $v = c_R^{II} = 1548$ m/s , a speed which is roughly five times smaller than their shear rupture counterparts.

Let us now turn our attention to the speed, v_c. Its significance became apparent through the theoretical work of Huang *et al.* [53] and Gao *et al.* [50]. They investigated the asymptotic nature of intersonic shear cracks propagating along a predetermined straight path in orthotropic solids, and determined the exponent of the stress singularity as follows [42]:

$$q = \frac{1}{\pi}\tan^{-1}\left[\frac{\mu_1}{\mu_2}\,\frac{c_{22}\left(c_{11}-\rho v^2+\mu_1^2 c_{66}\right)-c_{12}\left(c_{12}+c_{66}\right)}{c_{22}\left(c_{11}-\rho v^2-\mu_2^2 c_{66}\right)-c_{12}\left(c_{12}+c_{66}\right)}\,\frac{c_{11}-\rho v^2+\mu_2^2 c_{12}}{c_{11}-\rho v^2-\mu_1^2 c_{12}}\right], \quad (3.1)$$

where ρ is the mass density, c_{ij} are the in-plane moduli for an orthotropic solid,

$$\sigma_{11} = c_{11}\varepsilon_{11} + c_{12}\varepsilon_{22}, \quad \sigma_{22} = c_{12}\varepsilon_{11} + c_{22}\varepsilon_{22}, \quad \sigma_{12} = 2c_{66}\varepsilon_{12}, \qquad (3.2)$$

and x_1 denotes the fiber direction (i.e., direction of crack propagation), μ_1 and μ_2 are given by:

$$\mu_{1,2} = \sqrt{\frac{B^2 + 4c_{22}c_{66}\left(c_{11}-\rho v^2\right)\left(\rho v^2 - c_{66}\right)} \mp B}{2c_{22}c_{66}}}, \qquad (3.3)$$

and $B = c_{11}c_{22} - c_{12}^2 - 2c_{12}c_{66} - \left(c_{22}+c_{66}\right)\rho v^2$. It is evident from the above expressions that, except for one intersonic speed v_c, the exponent of stress singularity q is always less than one half such that the energy flux into the crack tip vanishes at all speeds within the intersonic regime with the exception of

$v = v_c$. At this speed, the energy flux is finite and positive, and the near tip deformation field resumes its original subsonic, square root singular, and radiation free nature. In particular, for an orthotropic solid, this critical speed is determined by q=1/2 [or equivalently the vanishing of the denominator inside the $\tan^{-1}$ function of equation (3.1)]. This gives the critical speed as:

$$v_c = \left(\frac{c_{11}c_{22} - c_{12}^2}{c_{66}(c_{12} + c_{22})} \right)^{1/2} c_s = \left(\frac{E_{11}}{\mu_{12}(1+\nu_{12})} \right)^{1/2} c_s \,, \qquad (3.4)$$

Where E_{11} and μ_{12} are the anisotropic elastic moduli, ν_{12} is an anisotropic Poissón's Ratio, and c_s is the shear wave speed. Exact definitions for $E_{11}, \mu_{12}, \nu_{12}$ and for c_s can be found in Huang *et al*. [53], or in Coker and Rosakis [52] together with their measured values for the fiber reinforced composite of the experiments. By using these values the speed v_c is calculated and it is found to be equal to 6600m/s. Moreover, this value is very close to the level identified experimentally as the lower bound of the oscillations discussed in relation to figure 24.

At this point it is important to note that for the case of isotropic materials the factor multiplying c_s in equation (3.4) becomes equal to $\sqrt{2}$ and the critical speed reduces to $v_c = \sqrt{2} c_s$. This is indeed the familiar speed that has consistently appeared in relation to intersonic shear crack propagation in isotropic solids discussed throughout this review article. Its physical importance and meaning is derived by the same energetic and stability arguments that have been discussed throughout section 2. In fact, as has also been shown by Gao *et al*. [50], the existence of radiation free transonic cracks can be demonstrated in relation to a much wider class of anisotropic solids.

The importance of using cohesive zone models to study intersonic rupture in orthotropic solids was once again emphasized by Broberg [55]. His analytical work shows that introducing cohesive structure into the crack tip removes the pathology of predicting zero energy flux into the intersonic crack tip. In fact, the cohesive zone model ensures the existence of a finite and positive energy flux throughout the intersonic regime. In a manner analogous to the isotropic cohesive models of section 2, the energy flux has a distinct maximum value at a

speed close, but not equal, to the critical speed v_c. Finally, cohesive theories have recently been used in conjunction with elaborate numerical schemes to study intersonic crack propagation. Noteworthy are Hwang and Geubelle's [56] contributions, which employed a spectral scheme to model mixed-mode failure of orthotropic materials. This work outlines the role of far-field mixity in determining favorable crack tip speed regimes. For the case of shear dominated crack growth, their speed history predictions are in excellent agreement with the results of Figure 24.

Finally, the existence of non-uniform, highly transient sliding processes trailing the tip of an intersonic shear crack have recently been verified numerically by Yu *et al.* [57]. In this calculation the unidirectional composite plates used by Coker and Rosakis [52] were modeled in three dimensions by means of finite elements. Material failure was allowed to proceed by satisfying a local decohesion law that was embedded in the boundaries between elements. The possibility of frictional contact was also taken into account while local temperature increases resulting from frictional dissipation were calculated at the appropriate locations. The equivalent two-dimensional problem was also studied by Dwivediy and Espinosa.

4. CONCLUSIONS

Extensive evidence of intersonic crack growth processes which occur in a variety of material systems containing preferable propagation paths have been presented in this article. Laboratory studies and theoretical and numerical models all strongly suggest that there are many underlying common elements in the physics governing shear decohesion. In particular it is clear, that irrespective of material systems, all intersonic shear crack propagations involve common properties such as:

1. Single or multiple shock wave formation,
2. Large-scale, non-uniform, frictional contact and sliding,
3. Similar mechanisms of nucleation or of subsonic to intersonic transition,
4. Similar intervals of preferable rupture speed stability.

The above commonalities are characteristic properties of dynamic shear crack propagation and are only relevant to the study of failure in solids that contain preferable crack-growth paths. In strictly homogeneous (monolithic)

solids, however, shear crack growth is unattainable. In addition, tensile crack growth is purely subRayleigh.

Table 1 below summarizes the maximum attainable crack tip speeds and illustrates the stable crack tip regimes in different material classes.

TABLE 1: Maximum attainable crack tip speed and stable crack tip regimes in different material classes. Only brittle solids are included

	Homogeneous Materials • Homogeneity in Elastic Behavior • *Homogeneity* in Fracture Toughness	**Materials with *Preferred* Crack Paths** • Homogeneity in Elastic Behavior • *Inhomogeneity* in Fracture Toughness (Fault)	
	Monolithic Rock, Ceramics, Glass, Brittle Polymers	Orthotropic Fiber Composites	Bonded Isotropic Solids
Mode-I			
Theory Limit	C_R	C_R	C_R
Observed Limit	$v_b \sim 0.35\text{-}0.5\ C_R$ (branching) stable steady state: $0 < v < v_b$	$\sim C_R$ Stable only at C_R	$\sim C_R$ Stable only at C_R
Mode-II	*INACCESSIBLE* (Asymmetric loading results in crack kinking along a locally mode-I direction)	Max observed: $C_L^{\parallel}$ Stable steady state: $v > v_c$ $v_c = \sqrt{\frac{E_1}{\mu_{12}(1+\nu_{12})}} C_s$	Max observed: C_L Stable steady state: $v > v_c$ $v_c = \sqrt{2} C_s$

Crack growth speed characteristics of both mode-I (tensile) cracks and mode-II (shear) cracks are compared in the two major rows. The two columns compare crack growth behaviour between strictly homogeneous (monolithic) materials and constitutively homogenous materials that have preferred crack paths. The column to the right also compares the crack speed behaviour of cracks in orthotropic and in bonded isotropic solids.

The case of inhomogeneous systems involving dissimilar bonded constituents, however, are not discussed in this article and are not represented in the above table. For such systems, research has not yet provided us with a clear-cut picture of maximum attainable crack tip speeds and preferable speed

stability regimes. Given the complexities involved in such systems; complexities due to the shear/normal traction coupling at the interface, it would not be surprising to conceive of the processes involved in the rupture of such systems as requiring a much more sophisticated level of analysis. Discussions of the developing literature on this subject can be found in the review paper by Rosakis *et al.* [46] and the recent work of Samudrala and Rosakis [47].

REFERENCES

1. Achenbach, J.D. (1973) *Wave Propagation in Solids.* North Holland, Amsterdam.
2. Freund, L.B. (1990) *Dynamic Fracture Mechanics,* 1st. Cambridge University Press, Cambridge.
3. Ravi-Chandar, K., Knauss, W.G. (1984) *Int. J. Fracture* **26**, 65.
4. Ravi-Chandar, K., Knauss, W.G. (1984) *Int. J. Fracture* **26**, 141.
5. Ramulu, M., Kobayashi, A.S. (1985) *Int. J. Fracture* **27**, 187.
6. Johnson, E. (1992) *Int. J. Fracture* **55**, 47.
7. Gao, H.J. (1993) *J. Mech. Phys. Solids* **41**, 457.
8. Fineberg, J., Marder, M. (1999) *Physics Reports* **313**, 2.
9. Ravi-Chandar, K., Knauss, W.G. (1999) *Comput. Sci. Eng.* **5**, 24.
10. Owen, D.M., Rosakis, A.J. and Johnson, W.L. (1998) Dynamic failure mechanisms in beryllium-bearing bulk metallic glasses. *Proceedings of the MRS Symposium on Bulk Metallic Glasses.*
11. Rosakis, A.J. (1993). In: *Experimental Techniques in Fracture*, pp. 327-425, Epstein, J. (Ed.).VCH Publishers, New York.
12. Broberg, K.B. (1999) *Cracks and Fracture*. Academic Press, London.
13. Broberg, K.B. (1989) *Int. J. Fracture* **39**, 1.
14. Broberg, K.B. (1996) *Materials Science* **32**, 80.
15. Washabaugh, P.D., Knauss, W.G. (1994) *Int. J. Fracture* **65**, 97.
16. Cotterell, B., Rice, J.R. (1980) *Int. J. Fracture* **16**, 155.
17. Nemat-Nasser, S., Horii, H. (1982) *J. Geophys. Res.,* **87** 6805.
18. Hutchinson, J.W., Suo, Z. (1992) *J. Geophys. Res.* **77**, 3796.
19. Freund, L.B. (1979) *J. Geophys. Res.* **84**, 2199.
20. Broberg, K.B. (1995) *Achiv. of Mech.* **47**, 859.

21. Broberg, K.B. (1996) *Mater. Sci.* **32**, 80.
22. Broberg, K.B. (1999) *Fatigue Fract. Eng. M.* **22**, 17.
23. Burridge, R. (1973) *Geophys. J. Royal Astro. Soc.* **35**, 439.
24. Andrews, D.J. (1976) *J. Geophys. Res.* **81**, 5679.
25. Ida, Y. (1972) *J. Geophys. Res.* **77**, 3796.
26. Palmer, A.C., Rice, J.R. (1973) *Proc. Royal Soc. Lond.* **A332**, 527.
27. Das, S., Aki, K. (1977) *Geophys. J. Royal Astro. Soc.* **50**, 643.
28. Day, S.M. (1982) *B. Seismol. Soc. Am.* **72**, 1881.
29. Johnson, E. (1990) *Geophys. J. Int.* **101**, 125.
30. Burridge, R., Conn, G. and Freund, L.B. (1979) *J. Geophys. Res.* **85**, 2210.
31. Broberg, K.B. (1994) *Geophys. J. Int.* **119**, 706.
32. Rosakis, A.J., Samudrala, O. and Coker, D. (1999) *Science* **284**, 1337.
33. Samudrala, O., Huang, Y. and Rosakis, A.J. (2002) Subsonic and intersonic shear rupture of weak planes with a velocity weakening cohesive zone, GALCIT-SM Report 00-2, Caltech, to appear in *J. Geophys. Res.*
34. Harris, R.A., Day, S.M. (1993) *J. Geophys. Res.* **98**, 4461.
35. Dugdale, D.S. (1960) *J. Mech. Phys. Solids* **8**, 100.
36. Barenblatt, G.I. (1962) *Adv. Appl. Mech.* **7**, 55.
37. Prakash, V., Clifton, R.J. (1993) Pressure-shear plate impact measurement of dynamic friction for high speed machining applications. *Proceedings of the 7th International Congress of Experimental Mechanics,* **SEM**, 568-596.
38. Prakash, V., Clifton, R.J. (1993) In: *Experimental Techniques in the Dynamics of Deformable Solids*, pp. 33-44. American Society of Mechanical Engineers, New York.
39. Prakash, V. (1998) *J. Tribol.-T ASME* **120**, 97.
40. Glennie, E.B. (1971) *J. Mech. Phys. Solids* **19**, 255.
41. Freund, L.B., Lee, Y.J. (1990) *Int. J. Fracture* **42**, 261.
42. Needleman, A. (1999) *J. Mech. Phys. Solids* **66**, 847.
43. Geubelle, P.H., Kubair, D.V. (2001) *J. Mech. Phys. Solids* **49**, 571
44. Abraham, F.F., Gao, H.J. (2000) *Phys. Rev. Lett.* **84**, 3113.
45. Abraham, F.F. (2001) *J. Mech. Phys. Solids* **49**, 2095.
46. Gao, H.J., Huang, Y. and Abraham, F.F. (2001) *J. Mech. Phys. Solids* **49**, 2113.
47. Huang, Y., Gao, H.J. (2001) *J. Appl. Mech.* **68**, 169.

48. Antipov, Y.A., Willis, J.R. (2001) Transient loading of a rapidly-advancing crack in a viscoelastic medium, Mathematics Reprint #01/06, The University of Bath.
49. Huang, Y., Gao, H.J. (2002) *J. Appl. Mech.* **69**, 76.
50. Gao, H.J., Huang, Y. Gumbsch, P and Rosakis, A.J. (1999) *J. Mech. Phys. Solids* **47**, 1941.
51. Guo, G., Wang, W., Huang, Y. and Rosakis, A.J. (2002) Suddenly accelerating or decelerating intersonic shear cracks, to appear in *J. Mech. Phys. Solids*.
52. Coker, D., Rosakis, A.J. (2001) *Philos. Mag. A* **81**, 571.
53. Huang, Y., Wang, W., Liu, C. and Rosakis, A.J. (1999) *J. Mech. Phys. Solids* **47**, 1893.
54. Barnett, D.M., Zimmerman, J.A. (2000) Non-radiating dislocations in uniform supersonic motion in anisotropic linear elastic solids. *Proceedings of the 6th International Conference on Integral Methods in Science and Engineering (IMSE 2000).*
55. Broberg, K.B. (1999) *Int. J. Fracture* **99**, 1.
56. Hwang, C., Geubelle, P.H. (2000) *CMES-Comp. Model Eng.* **4**, 45.
57. Yu, C., Pandolfi, A., Ortiz, M., Coker, D. and Rosakis, A.J. (2002) Three-dimensional modeling of intersonic shear crack growth in asymmetrically loaded unidirectional composite plates, GALCIT-SM Report 01-1, Caltech, to appear in *Int. J. Solids Struct.*
58. Rosakis, A.J., Samudrala, O. Singh, R.P. and Shukla, A. (1998) *J. Mech. Phys. Solids* **46**, 1789.
59. Samudrala, O., Rosakis, A.J. (2002) Effect of loading and geometry on the subsonic/intersonic transition of a bimaterial interface crack, GALCIT-SM Report 01-14, Caltech, to appear in *Eng. Fract. Mech.*

ACKNOWLEDGMENTS

AJR would like to thank the US Office of Naval Research (Grant # N00014-95-1-0453, Y.D.S. Rajapakse, Project Manager) for their consistent support of past and ongoing research on dynamic failure mechanics at Caltech. YH is grateful to the support from the US Office of Naval Research (Grant # N00014-01-1-0204, Y.D.S. Rajapakse, Project Manager).